Breast Cancer Research

Hypoxia inducible factor-1alpha promotes primary tumor growth and tumor-initiating cell activity in breast cancer

Breast Cancer Research 2012, **14**:R6 doi:10.1186/bcr3087

Luciana P Schwab (lschwab@uthsc.edu)
Danielle L Peacock (dpeacoc3@uthsc.edfu)
Debeshi Majumdar (debeshi_2005@yahoo.com)
Jesse F Ingels (jingels@uthsc.edu)
Laura C Jensen (ljensen3@uthsc.edu)
Keisha D Smith (ksmit185@uthsc.edu)
Richard C Cushing (rcushing@uthsc.edu)
Tiffany N Seagroves (tseagro1@uthsc.edu)

ISSN 1465-5411

Article type Research article

Submission date 14 June 2011

Acceptance date 7 January 2012

Publication date 7 January 2012

Article URL http://breast-cancer-research.com/content/14/1/R6

Hypoxia inducible factor-1α promotes primary tumor growth and tumor-initiating cell activity in breast cancer

Luciana P Schwab[1,2], Danielle L Peacock[1,2], Debeshi Majumdar[1], Jesse F Ingels[1], Laura C Jensen[1], Keisha D Smith[1], Richard C Cushing[1] and Tiffany N Seagroves[1,*]

[1]Center for Cancer Research and the Department of Pathology and Laboratory Medicine, The University of Tennessee Health Science Center, Cancer Research Building, 19 S. Manassas St., Memphis, Tennessee 38163, USA

[2]These authors contributed equally to the manuscript

[*]**Corresponding Author:** tseagro1@uthsc.edu

Abstract

Introduction: Over-expression of the oxygen-responsive transcription factor hypoxia inducible factor (HIF)-1alpha correlates with poor prognosis in breast cancer patients. The MMTV-PyMT (polyoma virus middle T) mouse is a widely utilized pre-clinical mouse model that resembles luminal breast cancer and is highly metastatic. Prior studies in the PyMT model demonstrated that HIF-1 is essential to promote carcinoma onset and lung metastasis, although no differences in primary tumor endpoint size were observed. Using a refined model system, we investigated whether HIF-1 is directly implicated in regulation of tumor-initiating cells (TICs) in breast cancer.

Methods: Mammary tumor epithelial cells (MTECs) were created from MMTV-PyMT mice harboring conditional alleles of *Hif1a*, followed by transduction *ex vivo* with either adenovirus-beta-galactosidase or Cre to generate wild type (WT) and HIF-1 null (KO) cells, respectively. The impact of HIF-1 deletion on tumor-initiating potential was investigated using tumorsphere assays, limiting dilution transplantation and gene expression analysis.

Results: Efficient deletion of HIF-1α reduced primary tumor growth and suppressed lung metastases, prolonging survival. Loss of HIF-1 led to reduced expression of markers of the basal lineage (K5/K14) in cells and tumors and of multiple genes involved in the epithelial to mesenchymal transition. HIF-1α also enhanced tumorsphere formation at normoxia and hypoxia. Decreased expression of several genes in the Notch pathway*, Vegf* and *Prominin-1* (CD133) were observed in response to HIF deletion. Immunohistochemistry confirmed that CD133 expression was reduced in KO cells and in tumorspheres. Tumorsphere formation was enhanced in $CD133^{hi}$ versus $CD133^{neg}$ cells sorted from PyMT tumors. Limiting dilution transplantation of WT and KO tumor cells into immunocompetent recipients revealed >30-fold enrichment of TICs in WT cells.

Conclusion: These results demonstrate that HIF-1alpha plays a key role in promoting primary mammary tumor growth and metastasis, in part through regulation of TICs. HIF-1 regulates expression of several members of the Notch pathway, CD133 and markers of the basal lineage in mammary tumors. Our results suggest that CD133, which has not been profiled extensively in breast cancer, may be a useful marker of TICs in the PyMT model. These data reveal for the first time that HIF-1 directly regulates breast TIC activity *in vivo*.

Introduction

A hallmark of most solid tumors, hypoxic regions are associated with resistance to radiation and chemotherapy [1, 2]. Oxygen tensions in advanced breast cancers can be as low as 0.1-1% O_2 [3], a range commonly used to model tissue hypoxia *in vitro*. The oxygen-responsive Hypoxia-Inducible Factor (HIF)-1α protein, a master regulator of the hypoxic response [4], is over-expressed in a variety of carcinomas and their metastases, including breast cancer [5]. A majority of DCIS and almost all poorly differentiated, invasive breast carcinomas over-express HIF-1α [6]. Moreover, HIF-1α promotes multiple steps of the metastasis program [7]. Either the over-expression of HIF-1α protein or the enrichment of a hypoxic gene signature in the primary tumor correlates with poor prognosis and decreased survival in breast cancer patients [8, 9].

Breast cancer cells that exhibit properties of cancer stem cells (CSCs), also referred to as tumor initiating cells (TICs), are more resistant than bulk tumor cells to therapeutic intervention, including radiation and DNA damaging drugs [10-12]. Hypoxic culture promotes self-renewal of several cell types, including neurospheres, hemapoietic stem cell cells (HSCs) and embryonic stem (ES) cells [13]. HIF-1 is also necessary *in vivo* for HSCs since its deletion causes stem cell exhaustion [14].

Accumulating evidence supports the hypothesis that stem cells and TICs exist in a hypoxic niche microenvironment [13]. The direct relationship of the hypoxic response to TIC activity has been demonstrated in adult glioma, human acute myeloid leukemia (AML) and murine lymphoma [15, 16]. In gliomas, expression of HIF2A was enriched, and knockdown of *HIF2A,* but not *HIF1A*, reduced TIC activity in patient xenografts [15]. In contrast, HIF-1 was found to be essential for maintaining TIC activity in a syngeneic rodent transplant model of lymphoma and in AML patient xenografts via regulation of the Notch pathway [16]. Interestingly, in gliomas, the TIC population was enriched via cell sorting based on the expression of a single cell surface

marker, CD133 (PROM1). PROM1, a transmembrane protein without a known ligand, is a hypoxia-responsive protein regulated by HIF-1 [17, 18].

Several studies have shown that the population of breast tumor cells with the ability to self-renew is enriched with the ability to initiate tumorigenesis *in vivo* [19-22]. Furthermore, TICs may drive metastasis [23, 24]. The MMTV-PyMT model is one of the most commonly utilized pre-clinical mouse models in breast cancer research since tumor latency is short and there is a high frequency of lung metastasis to the lung [25]. Whole-genome array profiling indicates that PyMT tumors most closely resemble the luminal B subtype of human breast cancer [26], although end-stage PyMT tumors are estrogen and progesterone receptor (ER/PR)-negative [25].

Moreover, the specific contribution of HIF-1α in regulating TICs in breast cancer remains undefined, particularly in the context of syngeneic rodent models that recapitulate the breast cancer microenvironment. It was previously shown that conditional deletion of *Hif1a* in PyMT+ tumors by crosses to mice expressing MMTV-Cre delayed the onset of palpable tumors, delayed the progression of hyperplasias to carcinomas and reduced lung metastases [27]. We have now created in an improved model system in which *Hif1a* is efficiently deleted in the mammary tumor epithelium via *ex vivo* viral transduction with Cre recombinase prior to the injection of mammary tumor cells to the cleared fat pads of recipient mice. Validating the use of a transplantation paradigm in lieu of intact transgenic mice, PyMT tumor cells transplanted serially into recipients exhibit similar morphology and gene expression profiles as the original tumors [28].

Using these novel HIF-1α wild type (WT) and null (KO) mammary tumor epithelial cells (MTECs), we demonstrate that HIF-1α prominently augments primary tumor growth and lung metastasis and accelerates relapse due to metastasis. Furthermore, we demonstrate for the first time that HIF-1α promotes mammary tumorsphere formation and enhances TIC frequency

in vivo, in part through regulation of the expression of markers associated with the basal lineage, the Notch pathway and CD133. Together, these data indicate that suppressing the hypoxic response may be beneficial not only to reduce primary tumor mass but also to suppress the breast TIC sub-population that may be ultimately responsible for patient relapse.

Materials and methods

Animals. Mice harboring two alleles of exon 2 of *Hif1a* flanked by *loxP* sites (double-*floxed, DF*) were provided by Dr. Randall Johnson (UCSD) on a mixed genetic background (129Sv;C57BL/6 [29]). *Hif1a* stock mice were first backcrossed to the FVB/Nj strain (Jax Labs) for 11 generations prior to breeding to MMTV-PyMT transgenic mice obtained from Dr. Kent Hunter (NCI), which had been previously backcrossed to the FVB/Nj strain. Lung metastasis is highly penetrant in the FVB/N background [30]. All procedures were approved by Instutitional Animal Care and Use Committee at the University of Tennessee Health Science Center.

Establishing HIF-1α wild type (WT) and knockout (KO) mammary tumor epithelial cells (MTECs). Several mammary tumors (>500 mm^3) were isolated from *Hif1a DF*; PyMT+ bi-genic females. Tumors were chopped with scapels then with razor blades and the paste digested with 1mg/mL collagenase type III (Worthington Biochemical, Lakewood, NJ) in RPMI media containing 5% FBS (5 mL/g tissue) for 2h at 37°C. Organoids were pelleted at 1100 rpm, washed 4 times with digestion buffer, and then plated into standard tissue culture plates in plating medium, as described in [31]. After 48-72 hours, the plating medium was switched to complete mammary epithelial cell growth medium [DMEM/F12, 5% FBS, 5 μg/mL insulin (Sigma), 10 ng/mL recombinant murine EGF (Invitrogen, Carlsbad, CA)]. At passage 6, MTECs were transduced with either Adenovirus ß–gal or Cre at a multiplicity of infection of 80 pfu/cell to

generate WT and KO MTECs, respectively. Adenoviral transduction was repeated again and the deletion efficiency between WT and KO MTECs was confirmed by both quantitative real-time PCR (qRT-PCR) and western blotting, using reagents presented in Additional file 1: Tables S1-S2. Post-adenoviral transduction, MTECs were subsequently weaned to medium containing only 2% FBS (DMEM/F12 + 2% FBS).

For sub-cultivation, cells were rinsed twice with Puck's A saline, then incubated for up to 60 min at 37℃ in a 3:1 solution of dispase II/0.25% trypsin reconstituted in Puck's A. No EDTA was utilized for subcultivating cells since treating cells with trypsin-EDTA changed tumor cell morphology from an epithelial (cuboidal) to a mesenchymal-like (spindle) appearance. All cells were passaged fewer than 30 times before use in tumorsphere or *in vivo* assays. Spent media was routinely tested for mycoplasma via the MycoAlert kit (Lonza, Basel, Switzerland).

All cells were grown either at normoxia in an air-jacketed $C0_2$ incubator (Sanyo; 5% $C0_2$), or at hypoxia (0.5% O_2; 5% $C0_2$) in a multigas incubator (Sanyo) in which N_2 gas displaces O_2. Cells were exposed acutely (≤6h) or chronically (>6h to several days) to hypoxia, and were removed from chronic hypoxic exposure only for brief periods to change medium.

For immunostaining of cultured cells, WT or KO cells passaged with dispase:trypsin were plated into tissue-cultured treated chamber well slides (BD Biosciences, Franklin Lakes, NJ), grown to 60-80% confluence and then post-fixed for 20 minutes at RT with 4% paraformaldehyde (PFA)/PBS followed by permeabilization with 0.5% Triton-X for 5 minutes. Cells stained with CD133 were not permeabilized. Primary antibodies to CD133, Troma-I (K8), cytokeratin 14 (K14), cytokeratin 5 (K5) were incubated overnight at 4℃ using dilutions in Additional file 1: Table S2. All cells were stained with DAPI prior to mounting with Vectasheild mounting medium (Vector Labs, Burlingame, CA).

Western blots. Insoluble material remaining after preparation of whole cell extracts (WCE) was re-extracted in high-salt (HS, 400mM NaCl) buffer, as in [32], except that the deubiquitinase

inhibitor N-ethylmaleimide (NEM) was added to a final concentration of 0.5μM. HS-WCE were resolved on 3-8% Tris-Acetate gels (1-10μg/lane; Invitrogen) and transferred to PVDF membrane prior to blocking with 5% milk and ECL-based detection of antibody complexes. All antibodies and dilution factors are listed in Additional file 1: Table S2.

Gene expression. Total RNA was prepared using RNABee reagent (Woodlands, TX) and RNA quality was confirmed by the Agilent 2100 Bioanalyzer (Santa Clara, CA) assay. RNA with a RNA Integrity Number (RIN) >9.0 was used to prepare cDNA using the High-Capacity cDNA Reverse Transcription kit (Applied Biosystems, Foster City, CA). qRT-PCR was performed using optimized primer and FAM-labeled probe sets designed with the Roche Universal Probe Library Assay Design Center software, as described in [33]. To control for cDNA input (40-80ng/reaction) when using cultured cells as the source of RNA, the C_p values were normalized based on the expression of the integrator complex subunit 3 (*Ints3*) gene, which is expressed at moderate levels in the mammary gland. This gene changes <20% between WT and KO cells cultured at normoxia or hypoxia or in WT and KO tumors by Illumina whole-genome expression arrays (T.N.S., personal observations). To compensate for any changes in epithelial content in whole tumors between genotypes, as only the tumor epithelium is deleted for *Hif1a*, *Ints3*-normalized C_p values were also normalized to *Krt18* (cytokeratin 18).

Cell growth and invasion assays. MTECs were grown at normoxic (ambient air; 5% $C0_2$) or hypoxic (0.5% O_2; 5% $C0_2$) culture in medium buffered with 25mM HEPES. The day before enumeration, either 350,000 cells/well in 6-well format (complete growth medium) or 100,000 cells/well in 12-well format (2% FBS medium) were seeded into multiwell plates. In all cases, medium was changed post-plating, but was not replinished for the duration of the experiment. Cells were harvested after culture for 0, 24, 48, 72 or 96h of culture at normoxia and hypoxia. All

cells were plated in triplicate or quadruplicate per genotype/oxygen tension/time point. Each replicate was counted by hemacytometer, and counts verified using an Accuri personal flow cytometer using the fast setting, after excluding cell debris.

For invasion assays, WT and KO MTECs that had been gradually weaned to medium supplemented with 0.5% FBS were cultured overnight in serum-free DMEM/F12 medium. The next day, 25,000 cells were plated onto control inserts or Matrigel-coated Transwell inserts (BD Biosciences) and attracted to wells containing complete growth medium (with 5% FBS). Cells were plated in triplicate per genotype/oxygen tension. The mean cell invasion index, corrected for random migration, was calculated as per manufacturer's instructions after 48 hours. Changes in invasion are expressed as a fold-change relative to the invasion index observed for WT cells cultured at normoxia (fold-change=1.0).

MTEC transplant into FVB recipients. MTECs dissociated to single cells with 0.05% trypsin/EDTA were counted by hemacytometer and diluted into HBSS. When transplanting into recipients at relatively low density (≤500 cells/gland), cells were diluted 1:1 (v:v) with growth-factor reduced Matrigel:HBSS; at higher densities cells were resuspened in HBSS alone. Cells (10μl) were kept on ice until injection to the right, inguinal mammary fat pad of 3-week old female FVB/Nj recipients (Jax Labs) using a 26G PT2 needle mounted to a Hamilton syringe, follwed by clearing of the endogenous epithelium. Recipients were palpated 1-2x/wk and outgrowths measured with digital calipers to calculate tumor volume, as in [27].

Tissue histology and immunostaining. Tumors were harvested from anesthetized mice and flash frozen in liquid nitrogen for preparation of RNA or protein, or were fixed in 10% neutral-buffered formalin (NBF) for 6h at RT for histology (H&E staining) and immunostaining. Paraffin-sections (5-7μm) were immunostained post antigen retrieval (1x citrate buffer) using the primary

anitbodies listed in Additional file 1: Table S2, followed by development with an ABC Elite kit and DAB Impact (Vector Labs). Alternatively, to prepare frozen sections suitable for CD133, Troma I, K14 and K5 immunofluorescent staining, anesthetized mice were intracardially perfused with 10% NBF. Tumor tissue was post-fixed for 10 minutes in NBF at RT prior to cryoprotection overnight at 4℃ in 30% sucrose/PBS, embedding in OCT and preparing 10 μm sections by cryostat. Sections used for visualizing the keratins were post-fixed for an additional 10 minutes in 10% NBF prior to 0.5% Triton-X permeabilization. All antibodies and staining conditions are listed in Additional file 1: Table S2.

Lung metastasis and survival studies. Lungs were either harvested from recipients at the same time as primary tumors (at a volume of ~1000 mm^3), eight weeks after primary tumor (500-750mm^3) resection or when recipients subjected to tumor resection were moribund, as indicated by body weight loss >15% and panting. Lungs were inflated with 10% NBF and post-fixed in NBF overnight. Paraffin-sections (7 μm) representing every 100 μm of lung tissue were obtained for each paraffin block and all sections were stained using H&E. The individual H&E-stained section containing the highest number of metastases per recipient, as evaluated by counting each slide under a light microscope at 50x magnification, was used to determine the grand mean of metastases per genotype.

Tumorsphere culture and immunostaining WT or KO MTECs were briefly trypsinized, washed and strained (40μm filter) to obtain single cells. The presence and viability of single cells was verified by viewing trypan blue stained cells by hemacytometer, only cells with a viability >90% were used in sphere assays. Single cells were resuspended in serum-free DMEM/F12 mammosphere media containing 20ng/mL mouse recombinant EGF, 20ng/mL bFGF, 1x B27 (all from Invitrogen) and 4 μg/mL heparin (Sigma, St. Louis, MO), as in [34].

Primary tumorspheres were derived by plating 30,000 single cells/well into 6-well ultralow adhesion dishes. Secondary and tertiary tumorspheres were plated at 5,000-10,000 cells/well and 2,000 cells/well, respectively. Dishes were cultivated at normoxia or hypoxia (0.5% O_2; $C0_2$) for 10-14 days prior to enumerating spheres. Individual spheres ≥100 μm were counted from each replicate well under a dissecting microscope (n≥12 wells/genotype/oxygen tension). The percentage of cells capable of forming spheres, termed the sphere formation efficiency (SFE), was calculated as follows: [(the number of spheres formed/ the number of single cells plated) x100]. End-point tumorspheres were collected from ultralow adhesion dishes, washed with PBS, then flash frozen for preparation of RNA or dried onto slides for 10-15 minutes at 37°C. Slides were post-fixed with 4% PFA/PBS for 15 minutes and immunostained with the antibodies indicated in Additional file 1: Table S2. All slides were stained with DAPI prior to mounting in either ProLong Fade Gold (Invitrogen) or Vectashield (Vector Labs) medium.

Tumor digestion and flow sorting. All mammary gland tumors used for flow sorting experiments were harvested from intact *Hif1a DF*; MMTV-PyMT+ (equivalent to HIF-1 WT) transgenic females at a size of >300mm^3 but <1500mm^3. Necrotic areas were removed from solid tumor tissue and solid tissue cut into small fragments with scissors. Tumor tissue was then weighed and chopped for 5 minutes with scapels followed by 5 minutes of chopping with razor blades to a fine paste. Tissue paste was digested in digestion buffer [DMEM/F12, 1x gentamicin, 1x antibiotic/antimycotic (Sigma), 300 U/mL collagenase type III (Worthington), 100 U/mL hyaluronidase (Sigma)] for 1-2h at 37°C at 125 rpm (10mL/g tissue). Digested tissue was pelleted by centifugation and the red blood cells lysed with a solution of 0.8% NH_4Cl:HBSS. In order to obtain single cells, organoids were further digested with 0.25% trypsin/EDTA for up to 10 minutes at 37°C and washed with serum containing medium to inactivate trypsin, followed by a final digestion for 10 minutes at 37°C in 5 mg/mL of dispase II (Roche)/Puck's A solution

containing 1 mg/mL DNase I (Roche). This cell suspension was passed through a 40 μm filter insert and this flow-through then passed through a flow cytometry tube with a 35 μm filter cap insert in order to further enrich for single cells. Viability post-digestion was routinely assessed by trypan blue staining; only cells with a viability of >85% were subjected to antibody staining.

Isolated single cells were resuspended to a density of up to 5 million cells/mL in flow buffer (FB: HBSS, 2% FBS, 10 mM HEPES) and incubated for 1 hour on ice with the biotin- or fluorophore-conjugated antibodies listed in Additional file 1: Table S2. These antibodies included a biotin-conjugated anti-mouse hematopoietc lineage panel, supplemented with anti-mouse CD31-biotin, anti-mouse CD133-PE and anti-mouse CD24-FITC, each at a 1:100 dilution. Secondary antibody incubation (SA-APC) in FB was performed for 30 minutes on ice. Post staining, cells were strained through a clean flow cytometry tube with a 35 μm filter cap. To determine cell viability, either SYTOXBlue (1 μm, Invitrogen) or 7-AAD (1 μg/mL, BD Biosciences) was added to each flow tube sample 10-20 minutes prior to cytometry.

Cells were subjected to cytometry profiling using the 100 μm nozzle at a sheath pressure of 20 p.s.i on a BD Biosciences FACSAria flow cytometer maintained by the UTHSC Flow Cytometry and Sorting Core equipped with violet (404 nm), blue (488 nm), green (532 nm) and red (635 nm) lasers, and applying FACSDiva software. All sample and collection tubes were maintained on ice. BD Biosciences CompBeads stained with either CD133-PE or CD24-FITC were used to set the compensation gates and cells stained with isotype-matched secondary antibodies were used as controls for staining specificity. Cells heat-killed for 30 minutes at 65°C were used to gate against dead cells positive for SYTOXBlue or 7-AAD. Lineage-negative (Lin^{neg}) cells were identified by gating against cells positive for the mouse lingeage panel+CD31. Since almost 100% of cells isolated from late stage carcinomas of the PyMT transgenic mouse were positive for CD24-FITC, as previously described [19], viable, Lin^{neg} mammary tumor cells were gated in a two-way sort for $CD133^{hi}$ versus $CD133^{neg}$ cells.

Sorted cells samples were collected directly on ice into 15mL conical tubes pre-coated with 20% FBS and a subset of collected cells were subjected to post-sort analysis to verify the purity and viability of the sorted populations. Sorted cell populations were immediately pelleted, washed to remove FBS and counted by hemacytometer prior to reconstitution in mammosphere medium and plating in 6-well ultralow adhesion dishes (Corning Life Sciences, Corning, NY) at the indicated density. FACSDiva plots were imported into FlowJo 7.0 (TreeStar) for data analysis and creation of histogram plots.

Limiting dilution transplantation. WT or KO MTECs were briefly trypsinized, washed with HBSS and serially diluted into 1:1 HBSS/Matrigel. Seven dilutions per genotype (500, 200, 100, 50, 25 or 10 cells/10μl) were introduced into the right inguinal, cleared fat pad of FVB/Nj recipients. Tumor-initiating potential was defined as the ability to form a palpable tumor mass >5mm diameter (~pea-sized). The estimated TIC frequency was calculated using Extreme Limiting Dilution Analysis (ELDA) software [35]. As a complementary approach, a Fisher's exact (Chi-square) test was also used to compare TIC activity between WT and KO cells at each cell density evaluated (Prism 4.0). Animals were palpated twice weekly until sacrifice.

Image acquisition. Western blots were scanned at 600dpi and imported into Photoshop. Digital images of immunostained or H&E-stained tissue sections and cells cultured on chamber-well slides were captured using a Leica DM6000 upright fluorescent microscope mounted with a CCD-cooled SPOT Insight digital camera and imported into Photoshop using Simple PCI software. All images between genotypes/conditions per experiment were digitally captured for the same exposure time. Immunostaining images were not digitally altered to reduce background or to adjust brightness or gain. Confocal images of spheres were captured every 0.75 μm with a Zeiss LSM210 microscope system. Appropriate gain and black level settings

were determined based on spheres incubated with secondary antibodiy alone. All images were captured using the same gain and exposure settings and upper and lower thresholds were set using the range indicator function. No additional background correction algorithms were applied. Digital slices were merged into a single composite image using Zeiss Zen software.

Results

A mammary tumor model with constitutively deleted HIF-1α

We observed that HIF-1α expression generally increases during progression in MMTV-PyMT mice, as previously observed in patients [6], thereby confirming that the MMTV-PyMT model is appropriate for these studies (Additional file 2: Figure S1). To generate a parental pool of MTECs, mammary tumors were isolated from *Hif1a floxed*; PyMT+ females (FVB/Nj background) and epithelial cells were transduced with ether Adenovirus-ß-gal or Cre to create HIF-1α wild type (WT) and null (KO) cell lines, respectively. Efficient *Hif1a* deletion was confirmed by real-time PCR and western blotting (Additional file 2: Figure S1).

During expansion, MTECs were weaned from complete growth medium to medium supplemented only with 2% FBS, as low serum medium was utilized to evaluate cell growth in [27]. The levels of HIF-1α detected by western blotting following acute (0-6h) or prolonged (>6h) hypoxia was determined using WT MTECs. On the initial day of hypoxic exposure, cells were 80% confluent prior to transfer to a hypoxic chamber for 24h, 12h, 8h, 6h and 3h prior to harvest. Cells from normoxic culture (t=0) were harvested at the same time as cells exposed to hypoxia for 24h. Similar to the profile observed in Hep3B cells [36], HIF-1α peaks by 3h of exposure to 0.5% 0_2 and by 24h, expression is attenuated to basal levels (Figure 1A). This decrease likely results because HIF-1α directly transcribes the prolyl hydroxylase (PHD) enzymes, enacting a negative feedback loop [37].

In contrast, when WT cells were cultured in presence of serum and EGF, HIF-1α levels were not attenuated by prolonged hypoxic exposure (Additional file 2: Figure S2), and, in fact, HIF-1α stabilization at hypoxia remained robust for at least 24h. As compared to the levels of HIF-1α expression observed in cells cultured in 2% FBS alone, EGF treatment increased HIF-1α levels ~4-fold at normoxia (t=0), and this up-regulation increased to >10- or >20-fold following 3h or 24h of hypoxic culture, respectively. The effect was not due to the differences in serum or insulin concentrations between culture media since WT cells cultured in 5% FBS + 5 μg/mL insulin without EGF expressed similar levels of HIF-1α as cells cultured in 2% FBS alone (data not shown). Overall, these results indicate that EGF is a potent regulator of HIF-1α expression in normoxic PyMT mammary tumor cells, as has been previously observed in SK-BR-3 and MCF-7 cells [38], and that under hypoxic conditions, EGF prolongs HIF-1α stabilization.

HIF-1 promotes cell growth and invasion

To determine whether the HIF-1α KO PyMT+ MTECs derived from *ex vivo* adenoviral transduction behave similarly *in vitro* as previously described [27], cell growth was compared in WT and KO cells cultured at normoxia and hypoxia. Cell growth was also compared for WT and KO cells cultured in complete or minimal (2% FBS only) growth medium. By 48h of culture, and then throughout the time course, there was a statistically significant difference between WT and KO cell number at normoxia or hypoxia in each medium formulation (Figure 1B), with fewer KO cells present than WT at each oxygen tension. Cells cultured in complete growth medium grew faster than in reduced serum. Often, in cells grown in 5% FBS + EGF, by 96h of culture at normoxia, more KO than WT cells were observed (Figure 1B), due to the acidic environment of the super-confluent WT cells, as reported in [39]. As expected, hypoxic exposure decreased the rate of growth for both WT and KO cells, although the difference between WT and KO cell density was the most striking following extended hypoxic exposure (≥72h).

Cells cultured in 2% FBS medium were gradually weaned to reduced serum (0.5% FBS) prior to use in invasion assays since immediate serum withdrawal resulted in massive cell death, even when cells had been routinely cultured in medium containing 2% FBS. Deletion of *Hif1a* reduced invasion at normoxia by 3.9-fold and by 3.5-fold at hypoxia (Figure 1C). In contrast, a significant induction of invasion by WT cells during hypoxia was not observed, as had been previously described in [27]. Although there was a trend towards increased invasion, the differences were not significant by ANOVA analysis. Likewise, there was no significant difference in the invasion potential of KO cells between normoxic and hypoxic culture.

Expression of basal markers is reduced in cultured KO cells

The expression of markers of the luminal (Troma-I, K8) and basal lineage (K5/K14) by WT and KO cells was evaluated by immunofluorescent staining of near confluent cells that were cultured overnight (12-14h) at normoxia or hypoxia (Figure 2). The majority of WT and KO MTECs cultured at normoxia (Figure 2a, 2e) and hypoxia (Figure 2i, 2m) stained with antibodies to K8 (Troma-I). This was expected since the PyMT model is a luminal-like model of breast cancer. However, fewer KO cells expressed K14 when cultured at either normoxia (Figure 2b vs. 2f) or hypoxia (Figure 2j vs. 2n). Hypoxic exposure down-regulated K14 expression in both WT and KO cells (Figure 2b vs. 2j, Figure 2f vs. 2n). Overall, fewer KO cells were dual-positive for K8 and K14 (yellow cells), suggesting a reduction in a bi-potent progenitor cell population in response to HIF-1 deletion. The most striking phenotype was that no K5+ cells could be detected in KO cells cultured at either normoxia (Figure 2d vs. 2h) or hypoxia (Figure 2l vs. 2p). Hypoxic induction of K5 mRNA has been previously reported in MCF-7 cells, [40], however, an increase in the number of K5+ cells was not apparent in PyMT WT cells exposed to hypoxia (Figure 2d vs. 2l).

Primary mammary tumor growth is HIF-1 dependent

To evaluate the contribution of HIF-1α to primary tumor growth in a syngeneic, transplant approach, WT or KO MTECs (50,000) were injected into a single cleared inguinal mammary fat pad of FVB/Nj recipient females. Single side injections were utilized in order to prevent one tumor from influencing the outgrowth of a contralateral tumor. There was a ~60% decrease in the wet weight and volume of KO tumors at week 8 post-transplant, when recipients bearing WT tumors required sacrifice due to institutional maximum tumor size recommendations (Figure 3A). Moreover, the rate of KO tumor growth was slower over the entire course of tumor development (Figure 3B). When fewer WT or KO cells were utilized to generate mammary tumors (500 cells/gland), there was a more pronounced delay in the ability of KO cells to form a tumor with a volume >500mm^3 (Figure 3C). The median time to form large tumors increased from 64 days for WT cells to 127 days for KO cells (Figure 3C).

To confirm that endpoint KO tumors did not express HIF-1α, western blotting was performed using extracts isolated from three randomly selected whole WT or KO tumors. Very low levels of HIF-1α were detected in KO end-stage tumors (Figure 3D). Residual expression was likely observed due to the presence of stromal components that are derived from the host recipients, such as tumor-associated macrophages. As expected, the expression of three classic HIF-1 target genes, *Vegf*, *Pgk1* and *Slc2A1* (*Glut1*), was reduced in KO tumors (Figure 3E). However, the gross histopathology of tumors was not affected by deletion of *Hif1a;* all tumors were poorly differentiated, solid adenocarcinomas as previously described for the PyMT transgenic mouse [25] (Additional file 2: Figure S3).

Because WT tumors were larger than KO tumors, they also exhibited more extensive necrosis than KO tumors. High-resolution, digitally-scanned, whole slides of H&E-stained tumors may be viewed using a link to a public database (refer to supplementary materials). Since a larger percentage of KO tumor cells were viable, it is not surprising that more Ki67 and caspase-3

positive cells were detected in KO tumors by immunostaining (Figures 3F, S4). Overall, these changes would be expected to have a zero net effect on KO tumor growth. In addition, as previously reported for late stage PyMT carcinomas [25], tumors derived from transplanted WT or KO cells did not exhibit any cells positive for ERα by immunostaining (Additional file 2: Figure S5).

HIF-1 promotes an EMT phenotype and regulates K5 expression in vivo

To determine if the expression of K5 and K14 was also reduced in KO tumors as in cultured cells, expression of K8, K14 and K5 was also evaluated by immunofluorescent staining of end-stage tumors harvested from FVB recipients bearing WT or KO tumors (n=4 tumors/cohort). The immunostaining pattern was compared to that observed in tumors harvested from intact PyMT transgenic mice. In contrast to results obtained in cultured cells, very few cells were dual positive for K8 and K14 in WT tumors. Furthermore, no cells positive for K5 or K14 were detected in any KO tumors (Figure 4A; n=4 tumors/genotype). In contrast, there were no obvious changes in the expression or localization of p63 detected by colorimetric immunostaining of paraffin embedded sections (Additional file 2: Figure S5; refer also to supplementary database of digitally scanned whole slides).

Real-time PCR analysis of RNA prepared from the same tumors for which sections were prepared for immunostaining revealed that K14 and K5 mRNA levels were reduced in KO tumors by 3.8- and 2.0 -fold, respectively. As expected based on the ability of hypoxia to promote an EMT phenotype through the Notch pathway [41], multiple core genes in the EMT signature were down-regulated in KO tumors compared to WT tumors, including Snail, Slug, Twist1, and fibronectin (Fn1), whereas expression of cytokeratin 18 was not affected by HIF-1 deletion (Figure 4B).

Constitutive *Hif1a* deletion represses metastasis and prolongs survival

Initially, metastasis was evaluated in WT or KO tumor recipients by harvesting lungs on the same day as the primary tumor. As recipients bore a single tumor, in contrast to the transgenic model in which all ten mammary glands become tumor-laden, very few metastases were present. The lungs from WT hosts exhibited a mean of two micrometastases, and the majority of lungs from KO hosts were devoid of metastases (Figure 5A).

One caveat of these data was that the tumors developed by the KO cells were 60% smaller than WT (Figure 5B). Therefore, to compare the effect on lung metastasis when WT and KO tumor volume was equivalent, the primary tumor was resected during a survival surgery procedure when tumors were at least 1.5 cm in diameter with a corresponding volume range of 500-750mm^3. Animals subjected to a survival surgery to resect the primary tumor were divided into two cohorts. In the first cohort, females were sacrificed 8 weeks post-surgery. WT tumor cells developed large macromets visible to the naked eye as well as several micrometastases visible by microscopic analysis, with a mean of 19 metastases per lung (Figure 5B, C). In contrast, lungs from KO tumor recipients contained 50% fewer metastases (Figure 5B, C), which were also smaller overall than the WT metastases. Furthermore, 50% of host mice transplanted with WT cells required sacrifice prior to the 8-week period, whereas all hosts harboring KO cells lived the full 8 weeks. Therefore, although KO MTECs retain the capacity to complete the full metastatic program, metastasis is significantly suppressed.

In the second cohort subjected to the tumor resection paradigm, recipients survived until moribund due to lung metastases (Figure 5D). Recipients bearing WT tumors succumbed to lung metastases sooner than KO recipients (Figure 5D). The median survival increased from 66.5 days for WT recipients to 88 days for KO recipients (n=14 WT, 21 KO; log-rank score, p <0.001). Furthermore, ~25% of mice implanted with KO tumors (5/21) lived beyond one year and did not develop any lung metastases, as evaluated by H&E staining of sections from the lungs.

Deletion of *Hif1a* decreases tumorsphere formation

To begin to determine if HIF-1α may play a role in regulating breast cancer stem cell activity, single WT or KO cells were placed into tumorsphere culture. All data shown in Figure 6 are representative experiments of several biological replicates. A summary of the fold change in sphere formation efficiency (SFE; or, the number of cells capable of forming spheres/total number of cells plated x 100) among biological replicate experiments is presented in Additional file 2: Figure S6. As shown in Figure 6A, the mean SFE was decreased by 4.1-fold in the primary, 2.2-fold in the secondary and 2.5-fold in the tertiary generations of spheres derived from KO cells, respectively. The mean SFE among biological replicate experiments varied from 0.06% to 1.55% for WT cells and 0.015% to 0.85% for KO cells. Variability in the sphere assay among biological replicates by over a $\log_{10}$ factor is not unusual [42]. More importantly, SFE within each experiment was always greater for WT cells than KO cells.

As shown in Additional file 2: Figure S6, the mean fold enrichment in SFE in WT cells was 4.3-fold for the primary generation (range of 2.85-7.23-fold), 4.1-fold for the secondary generation (range of 1.85-6.7-fold) and 2.61-fold for the tertiary generation (range of 2.1-2.79-fold). In each case, the mean fold change was determined from at least three biological replicates/genotype/generation. Because the WT and KO cells had been previously cultivated in monolayer in the presence of serum, the ability of HIF-1 to promote SFE was confirmed using tumor cells derived from freshly digested *Hif1a DF*; PyMT+ tumors originating in intact transgenic mice.

Following isolation from freshly digested tumors, single cells were immediately exposed in suspension (80 m.o.i for 2-3h) to Adenovirus-ß-gal or Cre, washed to remove viral particles and then plated at equal density into sphere culture conditions. Spheres derived from the primary generation were digested with trypsin, re-exposed to Adenovirus-ß-gal or Adenovirus-Cre in suspension (80 m.o.i for 2-3h) and plated for secondary generation spheres. Deletion

efficiency was determined for each generation by qRT-PCR of genomic DNA isolated from a fraction of cells collected at 72h post-plating, prior to formation of large tumorspheres.

In contrast to the established KO MTECs, not all *floxed* cells exposed 2-3h to Adenovirus-Cre were deleted for *Hif1a*. A mean deletion efficiency of 71% or 84% was observed following the first or second round of transduction with Adenovirus-Cre, respectively. Despite incomplete *Hif1a* deletion primary and secondary SFE was reduced in *Hif1a*-deleted cells by 2.53-fold and 2.30-fold at the primary and secondary generations, respectively (Figure 6B). The mean fold change in SFE between WT and *Hif1a* deleted (KO) cells among three biological replicates of this assay was 5.74-fold for the primary generation (range of 2.53-8.2-fold) and 4.38-fold for the secondary generation (range of 2.30-6.54-fold) (Additional file 2: Figure S6). These results confirm that the enrichment in SFE observed for WT cells previously cultured in monolayer with FBS was not an artifact due to culture conditions, and suggested that HIF-1α may promote breast TIC potential *in vivo*.

Sphere formation was also assayed after culture of WT and KO cells at normoxia or chronic hypoxia. Figure 6C presents data from one experiment in which there was a 2.28-fold reduction in KO SFE at normoxia and a 2.1-fold reduction in KO SFE at hypoxia, as compared to WT cells. Among biological replicates the mean fold reduction in KO SFE at normoxia was 3.26-fold (range of 2.20-6.15-fold) and 6.85-fold at hypoxia (range of 2.1-9.17-fold) (Additional file 2: Figure S6). Although there was a trend towards hypoxia increasing WT SFE (mean fold increase in SFE of 1.38, and a range of 1.17- to 1.70-fold, Additional file 2: Figure S6), the increase was not statistically significant in any independent experiment by ANOVA analysis. Changes in KO SFE between normoxia and hypoxia were also not significant (mean fold change of 0.94, and a range of 0.35-2.05-fold).

To determine if HIF-1α expression varied in spheres cultured acutely or chronically at hypoxia, HIF-1α expression was evaluated by western blotting of HS-WCE prepared from WT or

KO spheres exposed to prolonged hypoxia (≥ 4 days), or from WT or KO spheres that were initially grown in normoxic culture, but were then briefly exposed acutely to hypoxia (6h) prior to harvest (Additional file 2: Figure S7). In sphere culture conditions, HIF-1α was barely detectable in WT cells exposed to chronic hypoxia, whereas robust expression of HIF-1α was observed in WT cells exposed acutely to hypoxia. Therefore, in contrast to data obtained from monolayer cultured cells, EGF was not sufficient to stabilize HIF-1α expression when cells are grown constitutively at hypoxia in sphere culture.

One caveat of the tumorsphere assay is that spheres may be derived from aggregation of single cells, or even fusions of small spheres. The contribution of cell aggregation to sphere formation was not directly assessed in these experiments. However, the impact of aggregation on overall WT and KO SFE is presumed to be minimal since similar fold-changes in SFE between WT and KO cells were observed when cells were plated in sphere medium supplemented with 0.5% methylcellulose (data not shown), which acts as a physical barrier to impede cellular aggregation.

HIF-1α-dependent regulation of CD133 and the Notch pathway

Since CD133, Notch receptors and Notch target genes may be modulated by HIFs [16, 43, 44], expression of CD133, genes in the Notch pathway and classic HIF targets were evaluated in WT and KO tumorspheres by qRT-PCR. Figure 6D presents the mean fold reduction in gene expression observed in KO tumorspheres. Only genes that were consistently observed to be down-regulated across three biological replicate experiments are shown. Expression of *Notch4* was down-regulated an average of 7.24-fold, whereas expression of the Notch receptors *Notch1, Notch2 and Notch3* did not vary by more than 2-fold. The Notch ligand Delta-like-1 (*Dll1l*) was also down-regulated in KO spheres an average of 9.73-fold, and the transcription factors *Hey1* and Hey2 were down-regulated by 3.95-fold and 1.9-fold, respectively.

The *HEY* family of genes have been proposed to function as surrogate markers of Notch activity in multiple human breast cancer cell lines [45, 46].

Although the expression of the Jagged ligands has been reported to be hypoxia-inducible in breast cancer cell lines [45, 46], we were unable to confirm a consistent effect of HIF-1 on the expression of either *Jagged1* or *Jagged2* by tumorspheres. For example, the expression of *Jagged1* was up-regulated 3-fold in two experiments and down-regulated 3-fold in a third experiment, whereas the expression of *Jagged2* was observed to be up-regulated between 3-10-fold in two experiments and down-regulated 3-fold in a third experiment (data not shown). In addition, the expression of *Dll4*, *Hes1*, *Hes2* and *Vegf*, a direct HIF target gene, did not vary between WT and KO spheres by more than 1.5 fold. The most striking difference in gene expression was observed for *Prom1* (CD133), which was consistently down-regulated >9-fold in KO spheres (Figure 6D).

Based on qRT-PCR results, the expression of CD133 was then evaluated by immunostaining monolayer-cultured WT and KO MTECs grown at normoxia or hypoxia (6h) (Figure 7A). As compared to WT cells, CD133 positive cells were not readily detectable by immunostaining of KO cells following culture at normoxia or hypoxia (Figure 7A). These results were validated via flow cytometry following staining of WT and KO cells cultured at normoxia with CD133-PE-antibodies. As shown in Figure 7B, the expression of CD133 was reduced in KO cells by >9-fold. CD133 expression was also compared by immunostaining tumorspheres derived from WT and KO cells that were grown constitutively at normoxia (Figure 7C). As in cultured cells, the expression of CD133 was increased in WT spheres relative to KO spheres (Figure 7C), although in contrast to monolayer culture, CD133-positive cells were observed in KO spheres. Culture conditions influence the expression of CD133 mRNA levels since expression increased by a mean of 5-fold in WT cells spheres relative to the same passage of WT cells cultured in monolayer in 2% FBS (data not shown).

To test whether CD133 expression influences SFE, spheres were derived from the $CD133^{hi}$ or $CD133^{neg}$ sub-populations of late stage carcinomas arising in PyMT+ females. Live, lineage panel negative (Lin^{neg}), single cells were subjected to flow cytometry following staining with CD133-PE. Among replicate experiments, a range of ~5-12% of tumor epithelial cells were identified as highly positive for CD133-PE. A representative histogram plot is presented in Figure 7D, in which 5.99% of cells were isolated as the $CD133^{hi}$ fraction. An example of the gating strategy applied to sorting experiments is outlined in Additional file 2: Figure S8. The mean increase in SFE in the $CD133^{hi}$ sub-population compared to the $CD133^{neg}$ fraction among replicate experiments was >4.0-fold (a representative experiment is shown in Figure 7E), suggesting that CD133 may be a useful cell-surface marker to enrich for TICs in the PyMT model.

HIF-1α promotes TIC frequency *in vivo*

Based on the dramatic differences in growth rates of WT and KO tumors and the reduction in SFE by HIF-1 KO cells in tumorsphere assays, the ability of WT and KO cells to form tumors in recipients under limiting dilution transplantation conditions was evaluated. To permit estimation of TIC frequency due exclusively to loss of HIF-1 activity, TIC potential was compared using non-sorted WT or KO MTECs, in order to avoid the physical stress encountered during sorting that reduces cell viability and, therefore impacts calculation of TIC frequency [20]. The ability of WT or KO MTECs to form a palpable tumor mass of >5mm was evaluated using a broad range of cell dilutions (10-500 cells: 10, 25, 50, 100, 200 and 500) (Table 1).

At each cell density evaluated, there was a statistically significant enrichment in TIC activity in WT cells, indicated by the percentage of FVB/Nj recipients positive for a palpable tumor (Figure 8A, Table 1). ELDA analysis [35] revealed a 35-fold reduction in TIC frequency comparing KO to WT cells at day 36 post-transplant (Table 1). Data was also statistically

significant by Fisher's exact test (Table 1). The difference in TIC potential remained statistically significant at day 62 post-transplant (Additional file 2: Figure S9, Additional file 1: Table S3), with a 7.5 fold enrichment in TIC frequency in WT cells. One reason for the apparent decrease in the fold enrichment of TIC frequency at day 62 may be that the data from the 500 and 200 cell recipients were excluded in the ELDA analysis. All recipients in these cohorts were sacrificed at day 36 (Additional file 2: Figure S10) to compare histology and gene expression profiles of early-stage lesions. Notably, WT recipients in the 50 and 100 cell input cohorts required surgical intervention or euthanasia based on tumor volume by day 62 (Additional file 2: Figures S11-S12) whereas no intervention was required for KO recipients until day 96 post-transplant.

The mean volume of KO tumors derived under limiting dilution conditions was reduced, and this difference was maintained over several months. None of the KO tumors derived from transplantation of 50 or fewer cells exceeded a volume of 100 mm^3 by day 62 (Figure 8B). By day 112 post-transplant, 96% of recipients transplanted with 10 WT cells had developed measurable tumors whereas 55% of recipients transplanted with 10 KO cells had not (Additional file 1: Table S4), and, the mean tumor volume among the tumor-positive 10-cell KO recipients was <250 mm^3 (Additional file 2: Figure S12). Supplementary information summarizing the mean tumor volume per cohort and the percentage of recipients with measurable tumors at days 112 or 244 is presented in Additional file 1: Tables S4-S7 and Additional file 2: Figures S11-S12. The difference in TIC potential in the 10 cell cohort remained significant until day 244 (Additional file 1: Table S7), when all animals were euthanized.

HIF-1-dependent changes in gene expression were evaluated in early-stage (75-200 mm^3) WT and KO masses (n=5 tumors/genotype). Similar to results obtained from spheres, *Notch4*, *Hey1* and *Hey2* mRNA levels were decreased in KO tumors by 2.25-, 4.27-, and 2.3-fold, respectively (Figure 8C), whereas *Notch1-Notch3* mRNA levels decreased by less than 50%. All other genes in the Notch pathway that were previously profiled in spheres were not

differentially expressed among WT and KO tumors, except for *Vegf,* which was down-regulated by a mean of 7.3-fold. As observed in end-stage tumors, WT and KO *Glut-1* and *Pgk-1* mRNA levels were reduced in tumors <200mm^3.

By H&E staining, there were no gross changes in WT or KO tumor histopathology in recipients transplanted with 500 tumor cells. None of the KO masses within this cohort were detectable by manual palpation, but microscopic analysis of H&E-stained sections revealed lesions <5mm in 5/8 recipients. Since *Vegf* mRNA was differentially expressed, microvessel density was evaluated by Chalkley scoring following immunostaining with CD34. Decreased *Vegf* mRNA levels corresponded with a concomitant decreased mean Chalkley score in KO tumors (Figure 8D). In summary, deletion of *Hif1a* reduced TIC potential as well as neo-angiogenesis.

Discussion

Although the role of hypoxia and the HIFα transcriptional response in promoting tumor progression and metastasis is well established, the direct contribution of the HIF family to the regulation of TICs in breast cancer is unknown. HIF-1, rather than HIF-2, is the predominant regulator of the hypoxic response in breast cancer [47]; therefore, the effect of *Hif1a* deletion was determined in the MMTV-PyMT model of breast cancer. Herein, an *ex vivo* genetic deletion approach generated constitutive HIF-1α KO and control (WT) MTECs isolated from a pool of MMTV-PyMT tumors. One distinct advantage of this approach is that the MTECs are transplantable to immunocompetent hosts, preserving any host-derived effects on TIC potential following limiting dilution transplantation, in contrast to the xenograft of human cells into immunocompromised mice. We show for the first time that HIF-1α positively regulates TIC activity in breast cancer, as suggested via sphere-formation assays *in vitro* and validated through limiting dilution transplantation of WT and KO cells.

Additional advantages of the exogenous transduction and transplantation approach versus crosses to MMTV-Cre transgenic mice include avoiding the mosaic nature of MMTV-Cre expression, as not all epithelial cells harboring *floxed* alleles of *Hif1a* will undergo recombination [48], and avoiding the use of a mixed genetic strain background by utilizing mouse models backcrossed to a single strain (FVB/Nj). Since *Hif1a* deletion impairs cell proliferation [39], an effect we also observed in cultured KO MTECs (Figure 1B), incomplete recombination could permit non-targeted cells to outgrow the recombined (KO) cells. Additionally, it was not previously assayed whether the lung metastases originating in the MMTV-Cre-derived conditional KO females were derived from the recombined tumor cells, or were generated from cells that had escaped recombination [27]. Finally, mixed strain backgrounds may have introduced genetic modifier effects that would influence tumor incidence and lung metastasis. In particular, both tumor burden and lung metastasis in the MMTV-PyMT model are enhanced on the FVB/N background as compared to C57BL/6 [49].

In agreement with previous studies, we confirmed that HIF-1α promotes growth of MTECs cultured at hypoxia and enhances lung metastasis *in vivo* [27]. However, there were some differences observed between the two model systems. For example, we find that deletion of *Hif1a* repressed growth of cells at normoxia as well as at hypoxia (by 48h of culture). In addition, the magnitude of the decrease in KO cell invasion was similar whether cells were cultured at normoxia or hypoxia, whereas Liao et al. reported a difference only at hypoxia [27]. Finally, no statistically significant increase in invasion potential between WT cells cultured at normoxia and hypoxia was observed, as was reported in [27]. In contrast to observations from either PyMT model system in which *Hif1a* was deleted, shRNA-mediated knockdown of *HIF1A* in MDA-MB-231 cells did not significantly change cell number at either normoxia or hypoxia (1% O_2) [50]. It is possible that the effects of loss of HIF-1 activity on PyMT cell growth in monolayer culture would be attenuated if cells were cultured in higher serum, since MDA-MB-231 cells were cultured in

medium containing 10% FBS and PyMT cell lines were cultured in medium containing 2% or 5% FBS.

We further demonstrate that primary tumor growth and survival from distant metastases are dependent upon epithelial-cell intrinsic HIF-1α expression. In stark contrast to results obtained in [27], we find that HIF-1α plays a significant role in the control of primary PyMT-induced mammary tumor growth under either standard (50,000 cell input) or limiting dilution cell transplantation conditions (50-500 cell input). The mechanism for control of net mammary tumor growth by HIF-1 is unclear, although our data suggest that HIF-1-dependent control of TIC activity may be a primary mechanism to drive tumorigenesis. The significant changes in *Vegf* mRNA expression and microvessel density observed in early-stage KO tumors may also contribute to the phenotype by furthering restricting tumor growth once tumors are initiated. In agreement with our observations, a HIF-1-dependent effect on tumor growth has also been demonstrated recently in both MDA-MB-231 and MDA-MB-435 breast cancer xenografts [50, 51].

Characterization of the expression of luminal (K8/K18) and myoepithelial (K14/K5) lineage markers in WT and KO PyMT cells and tumors revealed that fewer KO cells co-expressed K8/K14 than WT cells, primarily due to loss of K14-positive cells. These results suggested that loss of HIF-1 activity corresponds with a reduction in bi-potent, stem-like cells in PyMT tumors. The most dramatic phenotype was the absence of K5-positive cells in KO cultures and the loss of both K14- and K5-positive cells in KO tumors. These data are of interest given the stratification of triple negative breast cancers (TNBCs) into non-basal-like or basal-like subtypes, based on the expression of both K5 and EGFR in tumors within the basal-like subtype [52].

TNBC patients with a basal-like classification have shorter disease-free or overall survival [53, 54] and tumors from TNBC patients with metastatic disease exhibit higher levels of K5 and EFGR [55]. A potential influence of HIF-1 on the ability of the K5 and EGFR biomarkers to predict disease-free survival in basal-like TNBC is intriguing in light of our observations that in cultured

cells, EGF stabilizes HIF-1α expression at normoxia and further potentiates hypoxia-inducible expression of HIF-1α. Although the PyMT model is classified as a luminal-like cancer [26], late stage tumors, such as the ones utilized to generate HIF-1 WT and KO cells, are ER- [25]; a sub-population of both WT cells and WT tumors were positive for K5.

It has also been observed in luminal breast cancer cell lines (T47D and MCF7), which contain sub-populations of ER-/PR-/K5+ cells, that the K5+ cells are enriched for TIC activity and are resistant to conventional chemotherapies as compared to ER+/PR+/K5- cells [56]. Of additional relevance to our results regarding the decreased expression of K5, K14 and markers of EMT, including *Slug*, by KO tumors in MCF7 cells, the hypoxia-dependent elevation in K5 mRNA levels occurs in a SLUG-dependent manner [40]. Furthermore, a statistically significant correlation existed between tumors with high *SLUG* expression and *PROM1* (CD133) expression, and these tumors also expressed high levels of carbonic anhydrase IX (CAR9) a HIF target gene [40].

Recent whole-genome expression profiling of breast cancers has revealed that the hypoxic response (predominantly through HIF-1), the epidermal growth factor receptor (EGFR) and signal transducer and activator of transcription (STAT)3 pathways are positively correlated together in TNBCs as compared to luminal cancers [57]. In support of a functional association between the HIF-1 and EGFR pathways in TNBCs, MDA-MB-231 cells treated with gefitinib exhibit down-regulation of HIF-1 transcriptional activity that corresponded with decreases in cell viability and migration, whereas resistance to cetuximab or lapatinib therapy was hypothesized to be due to the inability of either drug to down-regulate HIF-1 activity [56]. Taken together, these observations suggest that targeting the HIF pathway may beneficial to TNBC patients, particularly for those patients diagnosed with basal-like TNBC.

Based on the HIF-1-dependent control of CD133 expression in MTECs and tumorspheres, and the enrichment of sphere formation in the $CD133^{hi}$ vs. $CD133^{neg}$ populations, we have identified CD133 as a cell surface marker that may enrich for TICs in the PyMT model. Antibodies

to epitope 2 of CD133 (CD133/2) have been extensively utilized to enrich for TICs in other solid tumors, particularly in human colon cancer and gliomas. In contrast, in the normal mammary gland, CD133 is expressed by differentiated, ER+ luminal cells, and CD133+ cells exhibit lower regenerative capacity than CD133- cells [58]. Notably, deletion of *Prom1* in a knockout mouse model does not impair regenerative capacity of the normal mammary gland, but does reduce ductal branching during morphogenesis by increasing the ratio of luminal cells to basal cells [59]. Yet, in the NKI 295 dataset, *PROM1* expression levels were found to be lower in ERα+ tumors than in ERα-negative tumors [59]. The association of HIF-1α and *PROM1* expression in ER-negative breast cancers is not surprising given that hypoxia is a potent stimulator of ERα degradation [60, 61].

In contrast to observations in the normal mammary gland, Meyer and colleagues have recently shown that, in the context of ER-negative breast cancers, CD133 enriches for TICs when used in conjunction with CD49f (integrin α6) and CD44 [62]. Specifically, the $CD49f^{+}/CD44^{+}/CD133^{hi}$ population identified tumor cells with enriched sphere forming and xenografting potential. Likewise, CD133 has also been shown to enrich for TICs in the *Brca1* conditional mouse [21]. That a marker of a differentiated normal mammary epithelial cell could enrich for cells with TIC activity in the context of breast cancer is also supported by recent evidence from multiple laboratories that, in *BRCA1* basal-like tumors, the TIC population arises from the luminal lineage [63-65]. Interestingly, basal-like *BRCA1* tumors have been previously shown to over-express HIF-1α and higher HIF-1α levels correlated with decreased disease-free survival [66, 67]. Moreover, Proia et al. found that SLUG promoted a basal-like phenotype before and after transformation in *BRCA1* tumors [65], which is consistent with our observation that expression of *Slug* decreased by more than 3-fold in HIF-1 KO PyMT tumors, which were also K5/K14 negative.

Furthermore, accumulating evidence suggests that differentiated cells (lineage-restricted progeny) may re-acquire “stem-cell like” potential and tumor-initiating capacity, rather than following a strict linear hierarchy as originally proposed for the normal mammary gland. The plasticity involved in breast stem cell biology is emerging, as two independent groups have observed the spontaneous conversion of non-stem cells into stem cells [68, 69]. Likewise, results from recent lineage tracing experiments by the Blanpain laboratory have challenged the requirement for a bipotent stem cell in the post-natal normal mammary gland [70]. The authors further argue that, under the limiting cell conditions routinely used to document the regenerative capacity of a given cell population, the disruption of the normal luminal/myoepithelial cell ratio is sufficient to stimulate a unipotent myoepithelial progenitor cell to re-acquire bi-potent progenitor activity, which is normally restricted to the embryonic gland [70]. Yet, how, or if, this model derived from lineage tracing experiments will apply to TICs during breast tumorigenesis remains unknown.

One mechanism of HIF-1-dependent control of TIC may be through regulation of the Notch pathway. Interactions of HIF-1α with the Notch intracellular domain enhances the regulation of Notch transcriptional targets, such as the *HEY* genes, and promotes EMT in breast cancer [16, 71, 72]. In addition, in breast cancer, NOTCH1 and NOTCH4 have been positively correlated with stemness, and blocking antibodies to NOTCH4 reduce mammosphere formation [72]. In KO tumorspheres and early-stage KO tumors, decreased expression of several members of the Notch pathway, particularly *Notch4* and *Hey1*, was also observed. Changes in Notch4 are of particular interest as previous studies have shown that blocking NOTCH4 receptor activity inhibits tumor formation of xenografted breast cancer cells, whereas blocking NOTCH1 has less of an effect [72]. Although a relationship between hypoxia and NOTCH3 was previously described in breast cancer [73], no HIF-1-dependent changes in Notch3 were observed in our studies.

HIF-1α-dependent effects on sphere formation ability and TIC activity *in vivo* were observed using parental tumor cells, without first enriching for a putative CSC sub-population based on cell surface markers. One rationale for this approach is the lack of comprehensive information on the markers that define TICs in the PyMT model. However, in a similar PyMT tumor cell transplant paradigm, the population of CD24 (heat stable antigen)^{hi}/CD29(ß1-integrin)$^{+}$/CD61(ß3-integrin)$^{+}$ cells was found to significantly increase during progression, specifically at the transition from hyperplasia to carcinomas, with >90% of cells characterized as CD24^{hi}/CD29^{+}/CD61^{+} in late stage carcinomas. This population also had enhanced invasive potential *in vitro* [19]. More recently, the Visvader laboratory has shown that in cells derived from PyMT adenomas (early stage lesions), CD14 and c-kit along with CD49f/CD24 enriched for cells with colony-forming potential [74].

In addition, the physical stresses of flow sorting decrease cell viability, which, therefore, directly influences the estimated TIC frequency as determined through limiting dilution transplantation. As observed for the MMTV-Neu model, the TIC frequency of unsorted cells was 1/61, decreasing to 1/177 for cells enriched by sorting [20]. And, in cells isolated from adenomas in the PyMT model, the TIC frequency was estimated to be 1/556 for unsorted cells, whereas the TIC frequency in Lin^{neg} cells following sorting for CD24 was 1/648 [74]. In our hands, using unsorted cells isolated from late stage carcinomas of the PyMT model, we observed a TIC frequency of 1/82. It is possible that the TIC frequency in the PyMT model may vary based upon both the stage of progression and subtle differences in technical procedures among laboratories.

The specific cell surface markers that enrich for breast tumorsphere or TIC activity are also likely to vary in each mouse model. In the Balb/C p53$^{-/-}$ model, mammary tumor cells double-positive for CD24 and CD29 exhibit TIC activity [22], whereas in the MMTV-Neu model, Sca-1+ cells correlate with sphere formation [75], although CD61 does further enrich for TICs [20]. How HIF-1α directly impacts various tumor sub-populations as defined through flow

cytometry profiling of the known murine mammary stem cell markers, or if HIF-1α is preferentially expressed in a given population, requires further extensive investigation.

Conclusions

Tumor hypoxia profoundly impacts all aspects of tumorigenesis, including tumor growth, angiogenesis, metastasis and response to chemotherapy and radiation. Although HIF's effects are pleiotropic, evidence for the role of HIF-dependent TICs in controlling these phenotypes and the solid tumor stem cell niche is increasing. Notably, a recent report indicates that oxygen tension can profoundly influence TICs since repetitive cycles of hypoxia and reoxygenation promoted breast cancer cell lines to permanently acquire stem-like properties [76]. Our studies demonstrate that the hypoxic response, and HIF-1α specifically, is important for controlling breast cancer stem cell behavior through the regulation of CD133 and the Notch pathway. These data, along with previous observations that the HIFs directly mediate glioma, lymphoma and AML TIC activity [15, 16] suggest that attenuation of HIF activity may effectively eradicate TICs in a variety of cancers, leading to improved therapeutic response and overall survival.

We acknowledge that is possible that HIF-1 may simultaneously regulate activity of TICs and of differentiated cell lineages within a tumor. For example, HIF-1 may regulate breast TIC activity in a stem-like cell population expressing CD133, but HIF-1 activity may also be required by differentiated cells that may act to support the TIC through paracrine signaling, perhaps via a HIF-dependent secreted growth factor such as VEGF. Whether the EGFR pathway is required for HIF-1α-dependent regulation of TIC activity, particularly in basal-like TNBC also requires further investigation. Given the pleiotropic role of HIF-1 in tumorigenesis and metastasis, and the increasing evidence that stem cells may evolve *de novo* from non-stem cells, targeting both the TIC and non-TIC ("bulk") populations in breast cancer is likely necessary to successfully treat primary breast cancer and to prevent metastasis.

Abbreviations

PyMT, polyoma virus middle T; CSC, cancer stem cell; TIC, tumor-initiating cell; MTEC, mammary tumor epithelial cell; WT, wild type; KO, knockout; HSCs, hemapoietic stem cell cells; ES, embryonic stem; AML, acute myeloid leukemia; FBS, fetal bovine serum; WCE, whole cell extracts; NBF, neutral buffered formalin, 10%; PFA, paraformaldehyde, Lin, hematopoietic lineage panel; ELDA, extreme limiting dilution analysis; TNBC, triple negative breast cancer.

Competing interests

The authors declare that they have no competing interests

Acknowledgments

Drs. Randy Johnson (UCSD) and Dr. Kent Hunter (NCI) generously provided the *Hif1a* conditional allele (C57BL/6; 129SvEv) and MMTV-PyMT (FVB/Nj) mouse models, respectively. Dr. Yi Lu (UTHSC) provided assistance in amplifying adenovirus. Ms. Molly Jumper and Erica Harris provided excellent technical support. All Agilent and Roche LC480 assays were performed in the UTHSC Molecular Resource Center of Excellence. Drs. Tony Marion and Dan Rosson provided training at the UTHSC Flow Cytometry Laboratory. Drs. Heather LaMarca, Kaylee Schwertfeger and Cynthia Zahnow provided insightful comments. This work was supported by grants to TNS from the American Cancer Society (RSG-0702901-CNE, supporting TNS, LPS, LCJ and JI), the Department of Defense (W81XWH-09-1-0374, supporting TNS, DM and DLP), the NIH (CA-138488, supporting TNS, LPS and RCC), and the Gerwin and Maston Callison Bowld Cancer Research Funds at UTHSC (institutional startup funds awarded to TNS). The Zeiss 710 confocal microscope system was purchased by the UTHSC Neuroscience Institute with support from the NIH (NCRR 1S10 RR027221-01; PI, W. Armstrong). We also thank Dr. Lawrence T. Reiter for assistance with upright and confocal fluorescence microscopy. The Aperio ScanScope system was purchased by the UTHSC Department of Pathology with support from the NIH (NCRR 1S10RR025665-01; PI, C. Handorf). We also thank Dr. Anand Kulkarni and Ms. Crystal A. Stanton for providing assistance in digitally scanning whole slides and maintaining the publicly available database.

Authors' contributions

LPS participated in the study design, created the MTECs, carried out the animal studies, performed the tumorsphere assays using MTECs, western blotting and real-time PCR. She also performed the statistical analyses and assisted with drafting figures and the manuscript. DLP carried out the animal studies, flow cytometry sorting, the immunostaining, western blot and the real-time PCR assays, performed statistical analyses and assisted with drafting figures and editing the manuscript. LPS and DLP contributed equally to the study. DM performed the tumorsphere assays using freshly digested tumors and performed and analyzed real-time PCR data. KDS optimized immunostaining conditions and assisted with drafting figures. JFI performed and analyzed the cell invasion assays, genotyped the animals and cultured cell lines derived from animals. RCC and LCJ performed tumor resection surgeries, assisted with limiting dilution transplantation surgeries, prepared lung sections and counted metastases and analyzed metastasis data. TNS conceived of the study, created the study design, assisted with animal surgeries and data analysis and drafted figures and the manuscript. All authors read and approved the manuscript.

References

1. Rockwell S, Dobrucki IT, Kim EY, Marrison ST, Vu VT: **Hypoxia and radiation therapy: past history, ongoing research, and future promise**. *Current molecular medicine* 2009, **9**:442-458.
2. Cosse JP, Michiels C: **Tumour hypoxia affects the responsiveness of cancer cells to chemotherapy and promotes cancer progression**. *Anti-cancer agents in medicinal chemistry* 2008, **8**:790-797.
3. Vaupel P, Hockel M, Mayer A: **Detection and characterization of tumor hypoxia using pO2 histography**. *Antioxid Redox Signal* 2007, **9**:1221-1235.
4. Semenza GL: **Defining the role of hypoxia-inducible factor 1 in cancer biology and therapeutics**. *Oncogene* 2010, **29**:625-634.
5. Zhong H, De Marzo AM, Laughner E, Lim M, Hilton DA, Zagzag D, Buechler P, Issacs WB, Semenza GL, Simons JW: **Overexpression of hypoxia-inducible factor 1a in common human cancers and their metastases**. *Cancer Res* 1999, **59**:5830-5835.
6. Bos R, Zhong H, Hanrahan CF, Mommers E, Semenza GL, Pinedo HM, Abeloff MD, Simons JW, van Diest PJ, van der Wall E: **Levels of hypoxia-inducible factor-1a during breast carcinogenesis**. *J Natl Cancer Instit* 2001, **93**:309-314.
7. Gort EH, Groot AJ, van der Wall E, van Diest PJ, Vooijs MA: **Hypoxic regulation of metastasis via hypoxia-inducible factors**. *Curr Mol Med* 2008, **8**:60-67.
8. Chi JT, Wang Z, Nuyten DS, Rodriguez EH, Schaner ME, Salim A, Wang Y, Kristensen GB, Helland A, Børresen-Dale AL, Giaccia A, Longaker MT, Hastie T, Yang GP, van de Vijver MJ, Brown PO: **Gene expression programs in response to hypoxia: cell type specificity and prognostic significance in human cancers**. *PLoS Med* 2006, **3**:e47.
9. Dales JP, Garcia S, Meunier-Carpentier S, Andrac-Meyer L, Haddad O, Lavaut MN, Allasia C, Bonnier P, Charpin C: **Overexpression of hypoxia-inducible factor HIF-1alpha predicts early relapse in breast cancer: retrospective study in a series of 745 patients**. *Int J Cancer* 2005, **116**:734-739.
10. Atkinson RL, Zhang M, Diagaradjane P, Peddibhotla S, Contreras A, Hilsenbeck SG, Woodward WA, Krishnan S, Chang JC, Rosen JM: **Thermal enhancement with optically activated gold nanoshells sensitizes breast cancer stem cells to radiation therapy**. *Science translational medicine* 2010, **2**:55ra79.
11. Lacerda L, Pusztai L, Woodward WA: **The role of tumor initiating cells in drug resistance of breast cancer: Implications for future therapeutic approaches**. *Drug resistance updates : reviews and commentaries in antimicrobial and anticancer chemotherapy* 2010, **13**:99-108.
12. Creighton CJ, Li X, Landis M, Dixon JM, Neumeister VM, Sjolund A, Rimm DL, Wong H, Rodriguez A, Herschkowitz JI, Fan C, Zhang X, He X, Pavlick A, Gutierrez MC, Renshaw L, Larionov AA, Faratian D, Hilsenbeck SG, Perou CM, Lewis MT, Rosen JM, Chang JC: **Residual breast cancers after conventional therapy display mesenchymal as well as tumor-initiating features**. *Proceedings of the National Academy of Sciences of the United States of America* 2009, **106**:13820-13825.
13. Mohyeldin A, Garzon-Muvdi T, Quinones-Hinojosa A: **Oxygen in stem cell biology: a critical component of the stem cell niche**. *Cell Stem Cell* 2010, **7**:150-161.
14. Takubo K, Goda N, Yamada W, Iriuchishima H, Ikeda E, Kubota Y, Shima H, Johnson RS, Hirao A, Suematsu M, Suda T: **Regulation of the HIF-1alpha level is essential for hematopoietic stem cells**. *Cell stem cell* 2010, **7**:391-402.
15. Li Z, Bao S, Wu Q, Wang H, Eyler C, Sathornsumetee S, Shi Q, Cao Y, Lathia J, McLendon RE, Hjelmeland AB, Rich JN: **Hypoxia-inducible factors regulate tumorigenic capacity of glioma stem cells**. *Cancer Cell* 2009, **15**:501-513.
16. Wang Y, Liu Y, Malek SN, Zheng P: **Targeting HIF1alpha Eliminates Cancer Stem Cells in Hematological Malignancies**. *Cell Stem Cell* 2011, **8**:399-411.

17. Matsumoto K, Arao T, Tanaka K, Kaneda H, Kudo K, Fujita Y, Tamura D, Aomatsu K, Tamura T, Yamada Y, Saijo N, Nishio K: **mTOR signal and hypoxia-inducible factor-1 alpha regulate CD133 expression in cancer cells**. *Cancer research* 2009, **69**:7160-7164.
18. Soeda A, Park M, Lee D, Mintz A, Androutsellis-Theotokis A, McKay RD, Engh J, Iwama T, Kunisada T, Kassam AB, Pollack IF, Park DM: **Hypoxia promotes expansion of the CD133-positive glioma stem cells through activation of HIF-1alpha**. *Oncogene* 2009, **28**:3949-3959.
19. Kouros-Mehr H, Bechis SK, Slorach EM, Littlepage LE, Egeblad M, Ewald AJ, Pai SY, Ho IC, Werb Z: **GATA-3 links tumor differentiation and dissemination in a luminal breast cancer model**. *Cancer Cell* 2008, **13**:141-152.
20. Vaillant F, Asselin-Labat ML, Shackleton M, Forrest NC, Lindeman GJ, Visvader JE: **The mammary progenitor marker CD61/beta3 integrin identifies cancer stem cells in mouse models of mammary tumorigenesis**. *Cancer Res* 2008, **68**:7711-7717.
21. Wright MH, Calcagno AM, Salcido CD, Carlson MD, Ambudkar SV, Varticovski L: **Brca1 breast tumors contain distinct CD44+/CD24- and CD133+ cells with cancer stem cell characteristics**. *Breast cancer research : BCR* 2008, **10**:R10.
22. Zhang M, Behbod F, Atkinson RL, Landis MD, Kittrell F, Edwards D, Medina D, Tsimelzon A, Hilsenbeck S, Green JE, Michalowska AM, Rosen JM: **Identification of tumor-initiating cells in a p53-null mouse model of breast cancer**. *Cancer research* 2008, **68**:4674-4682.
23. Charafe-Jauffret E, Ginestier C, Iovino F, Wicinski J, Cervera N, Finetti P, Hur MH, Diebel ME, Monville F, Dutcher J, Brown M, Viens P, Xerri L, Bertucci F, Stassi G, Dontu G, Birnbaum D, Wicha MS: **Breast cancer cell lines contain functional cancer stem cells with metastatic capacity and a distinct molecular signature**. *Cancer Res* 2009, **69**:1302-1313.
24. Liu H, Patel MR, Prescher JA, Patsialou A, Qian D, Lin J, Wen S, Chang YF, Bachmann MH, Shimono Y, Dalerba P, Adorno M, Lobo N, Bueno J, Dirbas FM, Goswami S, Somlo G, Condeelis J, Contag CH, Gambhir SS, Clarke MF: **Cancer stem cells from human breast tumors are involved in spontaneous metastases in orthotopic mouse models**. *Proceedings of the National Academy of Sciences of the United States of America* 2010, **107**:18115-18120.
25. Lin EY, Jones JG, Li P, Zhu L, Whitney KD, Muller WJ, Pollard JW: **Progression to malignancy in the polyoma middle T oncoprotein mouse breast cancer model provides a reliable model for human diseases**. *Am J Pathol* 2003, **163**:2113-2126.
26. Herschkowitz JI, Simin K, Weigman VJ, Mikaelian I, Usary J, Hu Z, Rasmussen KE, Jones LP, Assefnia S, Chandrasekharan S, Backlund MG, Yin Y, Khramtsov AI, Bastein R, Quackenbush J, Glazer RI, Brown PH, Green JE, Kopelovich L, Furth PA, Palazzo JP, Olopade OI, Bernard PS, Churchill GA, Van Dyke T, Perou CM: **Identification of conserved gene expression features between murine mammary carcinoma models and human breast tumors**. *Genome Biol* 2007, **8**:R76.
27. Liao D, Corle C, Seagroves TN, Johnson RS: **Hypoxia-inducible factor-1alpha is a key regulator of metastasis in a transgenic model of cancer initiation and progression**. *Cancer Res* 2007, **67**:563-572.
28. Varticovski L, Hollingshead MG, Robles AI, Wu X, Cherry J, Munroe DJ, Lukes L, Anver MR, Carter JP, Borgel SD, Stotler H, Bonomi CA, Nunez NP, Hursting SD, Qiao W, Deng CX, Green JE, Hunter KW, Merlino G, Steeg PS, Wakefield LM, Barrett JC: **Accelerated preclinical testing using transplanted tumors from genetically engineered mouse breast cancer models**. *Clinical cancer research : an official journal of the American Association for Cancer Research* 2007, **13**:2168-2177.

29. Ryan HE, Poloni M, McNulty W, Elson D, Gassmann M, Arbeit JM, Johnson RS: **Hypoxia-inducible factor-1alpha is a positive factor in solid tumor growth**. *Cancer Res* 2000, **60**:4010-4015.
30. Hunter K, Welch DR, Liu ET: **Genetic background is an important determinant of metastatic potential**. *Nat Genet* 2003, **34**:23-24; author reply 25.
31. Rijnkels M, Rosen JM: **Adenovirus-Cre-mediated recombination in mammary epithelial early progenitor cells**. *J Cell Sci* 2001, **114**:3147-3153.
32. Ryan HE, Lo J, Johnson RS: **HIF-1 alpha is required for solid tumor formation and embryonic vascularization**. *Embo J* 1998, **17**:3005-3015.
33. Seagroves TN, Peacock DL, Liao D, Schwab LP, Krueger R, Handorf CR, Haase VH, Johnson RS: **VHL deletion impairs mammary alveologenesis but is not sufficient for mammary tumorigenesis**. *Am J Pathol* 2010, **176**:2269-2282.
34. Dontu G, Abdallah WM, Foley JM, Jackson KW, Clarke MF, Kawamura MJ, Wicha MS: **In vitro propagation and transcriptional profiling of human mammary stem/progenitor cells**. *Genes Dev* 2003, **17**:1253-1270.
35. Hu Y, Smyth GK: **ELDA: extreme limiting dilution analysis for comparing depleted and enriched populations in stem cell and other assays**. *J Immunol Methods* 2009, **347**:70-78.
36. Wang GL, Jiang B-H, Rue EA, Semenza GL: **Hypoxia-inducible factor 1 is a basic-helix-loop-helix-PAS heterodimer regulated by cellular 0_2 tension**. *Proc Natl Acad Sci* 1995, **92**:5510-5514.
37. Ginouves A, Ilc K, Macias N, Pouyssegur J, Berra E: **PHDs overactivation during chronic hypoxia "desensitizes" HIFalpha and protects cells from necrosis**. *Proceedings of the National Academy of Sciences of the United States of America* 2008, **105**:4745-4750.
38. Peng XH, Karna P, Cao Z, Jiang BH, Zhou M, Yang L: **Cross-talk between epidermal growth factor receptor and hypoxia-inducible factor-1alpha signal pathways increases resistance to apoptosis by up-regulating survivin gene expression**. *J Biol Chem* 2006, **281**:25903-25914.
39. Seagroves T, Ryan HE, Lu H, Wouters BG, Knapp AM, Thibault P, Laderoute KR, Johnson RS: **The transcription factor HIF-1 is a necessary mediator of the Pasteur effect in mammalian cells**. *Mol and Cell Biol* 2001, **21**:3436-3444.
40. Storci G, Sansone P, Trere D, Tavolari S, Taffurelli M, Ceccarelli C, Guarnieri T, Paterini P, Pariali M, Montanaro L, Santini D, Chieco P, Bonafé M: **The basal-like breast carcinoma phenotype is regulated by SLUG gene expression**. *J Pathol* 2007.
41. Sahlgren C, Gustafsson MV, Jin S, Poellinger L, Lendahl U: **Notch signaling mediates hypoxia-induced tumor cell migration and invasion**. *Proceedings of the National Academy of Sciences of the United States of America* 2008.
42. Visbal AP, LaMarca HL, Villanueva H, Toneff MJ, Li Y, Rosen JM, Lewis MT: **Altered differentiation and paracrine stimulation of mammary epithelial cell proliferation by conditionally activated Smoothened**. *Dev Biol* 2011, **352**:116-127.
43. Bar EE, Lin A, Mahairaki V, Matsui W, Eberhart CG: **Hypoxia increases the expression of stem-cell markers and promotes clonogenicity in glioblastoma neurospheres**. *The American journal of pathology* 2010, **177**:1491-1502.
44. Dontu G, Jackson KW, McNicholas E, Kawamura MJ, Abdallah WM, Wicha MS: **Role of Notch signaling in cell-fate determination of human mammary stem/progenitor cells**. *Breast cancer research : BCR* 2004, **6**:R605-615.
45. Chen J, Imanaka N, Griffin JD: **Hypoxia potentiates Notch signaling in breast cancer leading to decreased E-cadherin expression and increased cell migration and invasion**. *British journal of cancer* 2010, **102**:351-360.

46. Leong KG, Niessen K, Kulic I, Raouf A, Eaves C, Pollet I, Karsan A: **Jagged1-mediated Notch activation induces epithelial-to-mesenchymal transition through Slug-induced repression of E-cadherin**. *The Journal of experimental medicine* 2007, **204**:2935-2948.
47. Sowter HM, Raval RR, Moore JW, Ratcliffe PJ, Harris AL: **Predominant role of hypoxia-inducible transcription factor (Hif)-1alpha versus Hif-2alpha in regulation of the transcriptional response to hypoxia**. *Cancer Res* 2003, **63**:6130-6134.
48. Seagroves TN, Hadsell D, McManaman J, Palmer C, Liao D, McNulty W, Welm B, Wagner KU, Neville M, Johnson RS: **HIF1alpha is a critical regulator of secretory differentiation and activation, but not vascular expansion, in the mouse mammary gland**. *Development* 2003, **130**:1713-1724.
49. Lifsted T, Le Voyer T, Williams M, Muller W, Klein-Szanto A, Buetow KH, Hunter KW: **Identification of inbred mouse strains harboring genetic modifiers of mammary tumor age of onset and metastatic progression**. *Int J Cancer* 1998, **77**:640-644.
50. Zhang H, Wong CC, Wei H, Gilkes DM, Korangath P, Chaturvedi P, Schito L, Chen J, Krishnamachary B, Winnard PT Jr, Raman V, Zhen L, Mitzner WA, Sukumar S, Semenza GL: **HIF-1-dependent expression of angiopoietin-like 4 and L1CAM mediates vascular metastasis of hypoxic breast cancer cells to the lungs**. *Oncogene* 2011.
51. Wong CC, Gilkes DM, Zhang H, Chen J, Wei H, Chaturvedi P, Fraley SI, Wong CM, Khoo US, Ng IO, Wirtz D, Semenza GL: **Hypoxia-inducible factor 1 is a master regulator of breast cancer metastatic niche formation**. *Proceedings of the National Academy of Sciences of the United States of America* 2011, **108**:16369-16374.
52. Nielsen TO, Hsu FD, Jensen K, Cheang M, Karaca G, Hu Z, Hernandez-Boussard T, Livasy C, Cowan D, Dressler L, Akslen LA, Ragaz J, Gown AM, Gilks CB, van de Rijn M, Perou CM: **Immunohistochemical and clinical characterization of the basal-like subtype of invasive breast carcinoma**. *Clinical cancer research : an official journal of the American Association for Cancer Research* 2004, **10**:5367-5374.
53. Yamamoto Y, Ibusuki M, Nakano M, Kawasoe T, Hiki R, Iwase H: **Clinical significance of basal-like subtype in triple-negative breast cancer**. *Breast Cancer* 2009, **16**:260-267.
54. Cheang MC, Voduc D, Bajdik C, Leung S, McKinney S, Chia SK, Perou CM, Nielsen TO: **Basal-like breast cancer defined by five biomarkers has superior prognostic value than triple-negative phenotype**. *Clinical cancer research : an official journal of the American Association for Cancer Research* 2008, **14**:1368-1376.
55. Sutton LM, Han JS, Molberg KH, Sarode VR, Cao D, Rakheja D, Sailors J, Peng Y: **Intratumoral expression level of epidermal growth factor receptor and cytokeratin 5/6 is significantly associated with nodal and distant metastases in patients with basal-like triple-negative breast carcinoma**. *American journal of clinical pathology* 2010, **134**:782-787.
56. El Guerrab A, Zegrour R, Nemlin CC, Vigier F, Cayre A, Penault-Llorca F, Rossignol F, Bignon YJ: **Differential Impact of EGFR-Targeted Therapies on Hypoxia Responses: Implications for Treatment Sensitivity in Triple-Negative Metastatic Breast Cancer**. *PloS one* 2011, **6**:e25080.
57. Gatza ML, Kung HN, Blackwell KL, Dewhirst MW, Marks JR, Chi JT: **Analysis of tumor environmental response and oncogenic pathway activation identifies distinct basal and luminal features in HER2-related breast tumor subtypes**. *Breast cancer research : BCR* 2011, **13**:R62.
58. Sleeman KE, Kendrick H, Robertson D, Isacke CM, Ashworth A, Smalley MJ: **Dissociation of estrogen receptor expression and in vivo stem cell activity in the mammary gland**. *J Cell Biol* 2007, **176**:19-26.

59. Anderson LH, Boulanger CA, Smith GH, Carmeliet P, Watson CJ: **Stem cell marker prominin-1 regulates branching morphogenesis, but not regenerative capacity, in the mammary gland**. *Developmental dynamics : an official publication of the American Association of Anatomists* 2011, **240**:674-681.
60. Cooper C, Liu GY, Niu YL, Santos S, Murphy LC, Watson PH: **Intermittent hypoxia induces proteasome-dependent down-regulation of estrogen receptor alpha in human breast carcinoma**. *Clinical cancer research : an official journal of the American Association for Cancer Research* 2004, **10**:8720-8727.
61. Stoner M, Saville B, Wormke M, Dean D, Burghardt R, Safe S: **Hypoxia induces proteasome-dependent degradation of estrogen receptor alpha in ZR-75 breast cancer cells**. *Mol Endocrinol* 2002, **16**:2231-2242.
62. Meyer MJ, Fleming JM, Lin AF, Hussnain SA, Ginsburg E, Vonderhaar BK: **CD44posCD49fhiCD133/2hi defines xenograft-initiating cells in estrogen receptor-negative breast cancer**. *Cancer Res* 2010, **70**:4624-4633.
63. Lim E, Vaillant F, Wu D, Forrest NC, Pal B, Hart AH, Asselin-Labat ML, Gyorki DE, Ward T, Partanen A, Feleppa F, Huschtscha LI, Thorne HJ; kConFab, Fox SB, Yan M, French JD, Brown MA, Smyth GK, Visvader JE, Lindeman GJ: **Aberrant luminal progenitors as the candidate target population for basal tumor development in BRCA1 mutation carriers**. *Nat Med* 2009, **15**:907-913.
64. Molyneux G, Geyer FC, Magnay FA, McCarthy A, Kendrick H, Natrajan R, Mackay A, Grigoriadis A, Tutt A, Ashworth A, Reis-Filho JS, Smalley MJ: **BRCA1 basal-like breast cancers originate from luminal epithelial progenitors and not from basal stem cells**. *Cell Stem Cell* 2010, **7**:403-417.
65. Proia TA, Keller PJ, Gupta PB, Klebba I, Jones AD, Sedic M, Gilmore H, Tung N, Naber SP, Schnitt S, Lander ES, Kuperwasser C: **Genetic predisposition directs breast cancer phenotype by dictating progenitor cell fate**. *Cell Stem Cell* 2011, **8**:149-163.
66. van der Groep P, Bouter A, Menko FH, van der Wall E, van Diest PJ: **High frequency of HIF-1alpha overexpression in BRCA1 related breast cancer**. *Breast cancer research and treatment* 2008, **111**:475-480.
67. Yan M, Rayoo M, Takano EA, Fox SB: **BRCA1 tumours correlate with a HIF-1alpha phenotype and have a poor prognosis through modulation of hydroxylase enzyme profile expression**. *British journal of cancer* 2009, **101**:1168-1174.
68. Chaffer CL, Brueckmann I, Scheel C, Kaestli AJ, Wiggins PA, Rodrigues LO, Brooks M, Reinhardt F, Su Y, Polyak K, Arendt LM, Kuperwasser C, Bierie B, Weinberg RA: **Normal and neoplastic nonstem cells can spontaneously convert to a stem-like state**. *Proceedings of the National Academy of Sciences of the United States of America* 2011, **108**:7950-7955.
69. Gupta PB, Fillmore CM, Jiang G, Shapira SD, Tao K, Kuperwasser C, Lander ES: **Stochastic state transitions give rise to phenotypic equilibrium in populations of cancer cells**. *Cell* 2011, **146**:633-644.
70. Van Keymeulen A, Rocha AS, Ousset M, Beck B, Bouvencourt G, Rock J, Sharma N, Dekoninck S, Blanpain C: **Distinct stem cells contribute to mammary gland development and maintenance**. *Nature* 2011.
71. Gustafsson MV, Zheng X, Pereira T, Gradin K, Jin S, Lundkvist J, Ruas JL, Poellinger L, Lendahl U, Bondesson M: **Hypoxia requires notch signaling to maintain the undifferentiated cell state**. *Dev Cell* 2005, **9**:617-628.
72. Harrison H, Farnie G, Brennan KR, Clarke RB: **Breast cancer stem cells: something out of notching?** *Cancer Res* 2010, **70**:8973-8976.
73. Sansone P, Storci G, Giovannini C, Pandolfi S, Pianetti S, Taffurelli M, Santini D, Ceccarelli C, Chieco P, Bonafe M: **p66Shc/Notch-3 interplay controls self-renewal**

and hypoxia survival in human stem/progenitor cells of the mammary gland expanded in vitro as mammospheres. *Stem Cells* 2007, **25**:807-815.
74. Asselin-Labat ML, Sutherland KD, Vaillant F, Gyorki DE, Wu D, Holroyd S, Breslin K, Ward T, Shi W, Bath ML, Deb S, Fox SB, Smyth GK, Lindeman GJ, Visvader JE: **Gata-3 negatively regulates the tumor-initiating capacity of mammary luminal progenitor cells and targets the putative tumor suppressor caspase-14**. *Molecular and cellular biology* 2011.
75. Grange C, Lanzardo S, Cavallo F, Camussi G, Bussolati B: **Sca-1 identifies the tumor-initiating cells in mammary tumors of BALB-neuT transgenic mice**. *Neoplasia* 2008, **10**:1433-1443.
76. Louie E, Nik S, Chen JS, Schmidt M, Song B, Pacson C, Chen XF, Park S, Ju J, Chen EI: **Identification of a stem-like cell population by exposing metastatic breast cancer cell lines to repetitive cycles of hypoxia and reoxygenation**. *Breast cancer research : BCR* 2010, **12**:R94.
77. Seagroves TN, Lydon JP, Hovey RC, Vonderhaar BK, Rosen JM: **C/EBPbeta (CCAAT/enhancer binding protein) controls cell fate determination during mammary gland development**. *Mol Endocrinol* 2000, **14**:359-368.

Figure legends

Figure 1. Effect of HIF-1α deletion upon growth and invasion. A. WT MTECs grown to 80% confluence were subjected hypoxia culture for the indicated number of hours for up to 24h, or cells were continued to be cultured at normoxia, such that the t=0 sample was harvested on the same day as the t=24h hypoxic sample. HS-WCE were resolved on 3-8% Tris-Acetate gels and blotted to PVDF membrane, which was divided horizontally at approximately 60kDa. The top half of the blot was blotted for HIF-1α and the lower portion was blotted for lamin (loading control) to avoid the need to strip and reprobe the blot. B. Growth curve of WT and KO MTECs cultured at normoxia (Nor) or hypoxia (Hyp) in growth medium supplemented with 5% FBS + EGF (left panel) or with 2% FBS (right panel). For cells grown in 5% FBS + EGF, a representative graph is shown, in which the mean cell number ± S.E.M. per time point of quadruplicate wells per genotype/oxygen tension is plotted per time point. For cells grown in 2% FBS, the grand mean of cell number ± S.E.M. is presented, calculated as an average of the mean cell number observed per replicates per time point, as observed in three replicate

experiments. All data was analyzed by two-way ANOVA (*p<0.05). C. The mean fold-change in invasion was normalized to the invasion index observed for WT cells cultured at normoxia (FC=1.0). Data represent the mean fold change in invasion observed in three independent experiments. All columns were compared to each other using one-way ANOVA analysis with a Bonferroni post-test, *p<0.05.

Figure 2. Loss of basal marker expression in cultured HIF-1 KO cells. WT or KO cells were plated onto tissue-cultured treated slides and grown to sub-confluence, at which time a subset of cells were exposed overnight to hypoxic culture or remained under normoxic culture. Cells were co-stained with Troma-I (K8, green) and K14 (red) (panels a-c, e-g, i-k and m-o) or with K5 alone (panels d, h, l, p); all slides were counterstained with DAPI. Images were captured at 200x magnification (scale bar indicates 50 μm).

Figure 3. Deletion of *Hif1a* decreases primary tumor growth. A. WT or KO cells (50,000) were transplanted into FVB/Nj recipients. All tumors were harvested at day 56 to evaluate tumor weight, volume and burden (% tumor weight/total body weight) (n=10 recipients/genotype, p <0.05, unpaired student's t-test). B. The growth rate of WT and KO tumors at 50,000 cells input. Best-fit curves were established based on a polynomial fit algorithm in Prism 4.0. Data in A-B are representative of seven independent experiments (>60 recipients/genotype). C. When 500 WT and KO cells are input, the median time to 50% of recipients to develop tumors >500 mm^3 is 64 days for WT and 127 days for KO (n=14 recipients/genotype, p <0.001, log-rank test). D. Western blotting for HIF-1 α in three independent tumors (500-750 mm^3) per genotype; WT and KO cells that were cultured 6h at hypoxia serve as positive and negative controls (CRM, cross-reactive material). E. Mean fold-change ± S.E.M in expression of HIF-1 targets in KO tumors as determined by qRT-PCR (n=5 tumors/genotype). F. An increase in Ki67+ cells in KO tumors is

balanced by an increase in caspase-3+ cells (n=5 tumors/genotype, *p <0.05, student's t-test). Representative images of immunostaining are included in Additional file 2: Figure S4.

Figure 4. Loss of cells expressing K14 or K5 in HIF-1 KO tumors is accompanied by a reduction in the expression of markers of EMT. A. Frozen sections were prepared from tumors harvested from PyMT+ transgenic mice, or from WT and KO tumors harvested from FVB recipients. All tumors were ≥500 mm^3 in volume. Sections were co-stained with antibodies to K14 (red) and K8 (green) or K5 (red) alone, and counterstained with DAPI. Images were captured at 200x magnification; the scale bar represents 50 μm. B. The mean fold-change ± S.E.M. in gene expression observed in end-stage KO tumors of K14 and K5 mRNAs, as well multiple markers of EMT, as determined by real-time PCR performed using primers and probes in Additional file 1: Table S2 (n=5 tumors/genotype). The mean ± S.E.M. of biological replicates is graphed. The expression of Snail, Slug, Twist1, Fn1, K14 and K5 mRNAs was reduced in KO tumors compared to WT tumors, however, the expression of K18 varied less than 20% between genotypes.

Figure 5. HIF-1α expression in tumor epithelium is required for metastasis. A. Mean number of micrometastases ± S.E.M observed when lungs are harvested at the same time as the primary tumor (>1,000 mm^3) (n=9 WT, 14 KO recipients, *p< 0.05, unpaired student's t-test). B. Enhancement of lung metastases when WT and KO primary tumors are surgically resected at equivalent volumes (500-750 mm^3), followed by 8 weeks of survival (n=32 WT, 22 KO recipients, *p <0.05 student's t-test). C. Representative images of lungs harvested from WT or KO MTEC recipients 8 weeks after tumor resection (50x magnification). D. The impact of HIF-1α expression in tumor cells on the survival of recipients following tumor resection. A subset of animals subjected to primary tumor resection was allowed to survive until moribund due to

metastasis. The morbidity hazard ratio is 3.78 times higher when hosts bear WT tumors (n=14 WT, 15 KO hosts, log-rank test, p=0.00039, 95% C.I. =1.53-9.31).

Figure 6. HIF-1α promotes tumorsphere formation in cultured cells and in freshly isolated tumor cells independent of oxygen tension. A. Representative experiment in which the mean sphere formation efficiency (SFE) ± S.E.M. was determined when WT and KO cells were cultured in tumorsphere culture conditions. Tumorspheres ≥100 μm were scored positive, and the mean SFE (the percentage of cells capable of forming spheres per total number of single cells plated) per experiment (n≥12 wells/genotype; p<0.05, unpaired student's t-test) was determined at each of the primary, secondary and tertiary generations of spheres. A summary presenting the mean fold enrichment in WT SFE observed among biological replicates is included in Additional file 2: Figure S6. B. A representative experiment in which the mean primary and secondary SFE ± S.E.M. was determined when single cells were isolated from mammary tumors of *Hif1a DF*; MMTV-PyMT+ mice followed by immediate adenoviral transduction (n≥12 wells/genotype; p<0.05, unpaired student's t-test). C. Comparison of SFE when WT or KO cultured cells were subjected to normoxia or chronic hypoxia. Immediately following plating of single cells, dishes were cultured at normoxia or hypoxia throughout the duration of the experiment, therefore, cells were exposed to chronic hypoxia. The graph presents mean SFE obtained from the secondary generation of spheres (n≥12 wells/genotype). Differences among columns were analyzed by ANOVA, *p<0.05. D. The mean fold change in gene expression observed in KO tumorspheres evaluated by qRT-PCR. The grand mean fold change ± S.E.M. was determined from three independent experiments; cDNA was derived from three preparations of WT and KO secondary spheres grown in 6-well format and pooled at experiment endpoint to prepare total RNA (n=3 pools of spheres/genotype). The mean expression of *Notch 4* (N4), *Dll1*, *Hey1*, *Hey2* and *Prom1* (CD133) was reduced in KO

tumorspheres by greater than 1.5-fold, whereas the mean expression of *Notch1*, *Notch2*, and *Notch3* (N1-N3), or *Vegf* did not vary by more than 50% between genotypes. The decreased expression in KO tumorspheres is indicated as a negative fold-change.

Figure 7: CD133 expression in PyMT MTECs is regulated by HIF-1. A. Sub-confluent WT or KO cultured cells were exposed to acute hypoxia (6h), then immunostained for CD133 (green) and counterstained with DAPI. Images were captured at 200x magnification; the scale bar represents 50 μm. B. Representative CD133-PE staining profiles of WT (red histogram) and KO (blue histogram) cells cultured at normoxia and subjected to FACS analysis. The isotype only antibody control is also plotted (green histogram). The percentage of cells that were CD133 positive was determined based on the live, singlet, Lin^{neg} parent population using FlowJo. C. Secondary WT or KO tumorspheres cultured at normoxia were harvested at study endpoint from ultralow adhesion wells, dried onto glass slides, stained with CD133-PE, counterstained with DAPI and imaged by confocal microscopy. The highlighted area (white boxes) shows a higher magnification image, which demonstrates that CD133 is localized to the cell surface/membrane. D. Histogram of CD133-PE (red) in the live, singlet, Lin^{neg} parent population of cells isolated from tumors that arose in the PyMT transgenic mouse, as compared to the isotype antibody control (green); approximately 6% of cells were defined in this experiment as $CD133^{hi}$. D. A representative experiment showing the mean SFE/well ± S.E.M of $CD133^{hi}$ vs. $CD133^{neg}$ sub-populations that were isolated by flow sorting and cultured at normoxia at a density of 10,000 cells/well in 6-well format ($n \geq 8$ wells/genotype, unpaired student's t-test). The SFE was determined as the percentage of cells capable of forming spheres per the total number of single cells plated.

Figure 8. HIF-1α regulates tumor-initiation potential *in vivo*. A. Evaluation of the percentage of recipients (number of recipients positive for a palpable mass/number of recipients successfully transplanted x100) that developed a tumor mass by day 36 post-injection of unsorted WT and KO tumor cells. The asterisks indicate a significant difference between genotypes for a given cell density by Fisher's exact test. B. Comparison of WT and KO mean tumor volume ± SEM over time when 10, 25 or 50 cells are injected into the mammary fat pad. C. The mean fold change ± S.E.M. in gene expression profiles of early-stage tumor masses was evaluated by qRT-PCR; all genes displayed were down-regulated in KO tumors as compared to WT tumors (n=4 tumors/genotype/experiment).

Table 1: **Estimation of TIC frequency of HIF-1α WT and KO MTECs**

	Genotype of MTECs		
Number of cells injected	**HIF-1α WT** **Tumor-positive**	**HIF-1α KO** **Tumor-positive**	**Fisher's exact test**
500	78% (7/9)	0% (0/8)	*p*=0.0023
200	90% (9/10)	10% (1/10)	*p*=0.0011
100	77% (10/13)	9% (1/11)	*p*=0.0003
50	69% (11/16)	6% (1/16)	*p*=0.0006
25	30% (6/20)	0% (0/20)	*p*=0.0202
10	35% (8/23)	0% (0/22)	*p*=0.0038

Estimated TIC freq. by ELDA (95% C.I.)	**HIF-1α WT** 1/82 (1/57-1/117) *p* value, $5.79e^{-21}$	**HIF-1α KO** 1/2915 (1/925-1/9193)

Table 1. Frequency of tumors following limiting dilution transplantation of WT or KO MTECs. The number of tumor-positive recipients/total number of recipients at day 36 post-

transplant is indicated as well as the *p*-value of the Fisher's exact test between genotypes for each cell density tested. The estimated frequency of TICs was determined using the publicly available ELDA software.

Additional files.

Additional file 1:

Table S1. Primers and Roche Universal Probe Library (UPL) FAM-labeled probes utilized in quantitative real-time PCR (qRT-PCR) assays.

Table S2. Primary antibody source and dilution factors utilized in western blotting, immunohistochemistry (IHC), immunofluorescence (IF) and FACS.

Table S3. Frequency of tumors in recipient mice at day 62 after limiting dilution transplantation.

Table S4. Frequency of tumors in recipient mice at day 112 after limiting dilution transplantation.

Table S5. Summary of the percentage and total number of recipients bearing small tumors at day 112 post-transplant.

Table S6 Frequency of tumors in recipient mice at day 244 after limiting dilution transplantation.

Table S7 Summary of the percentage and total number of recipients bearing small tumors at day 244 post-transplant.

Additional file 2

Figure S1. **HIF-1α expression increases during tumor progression in the MMTV-PyMT model and confirmation of HIF-1α deletion.** HS-WCE protein extracts were prepared from two individual transgenic MMTV-PyMT female mice (FVB/Nj strain) between 6-9 weeks of age. By palpation, each mouse had at least one mammary gland with hyperplastic (HP; palpable as grainy), early carcinoma (EC, <250mm^3) or late carcinoma (LC, >500mm^3) lesions, which was expected, since tumor progression among glands is asynchronous in this model. Two independent glands (one from each mouse) per stage were utilized to prepare HS-WCE for western blotting. As shown, HIF-1α expression generally increases during progression, and is most abundant in late stage carcinomas. Included as controls are HS-WCE prepared from WT and KO MTECs grown to 80% confluence followed by hypoxic exposure for 6h at 0.5% O_2. A

cross-reactive band (CRM) at ~76kDa was detectable when using lot E2 of the Novus Biologicals anti-mouse HIF-1α primary antibody (NB 100-479). KO cells were transduced twice with Adenovirus-Cre in monolayer culture at 80-100 p.f.u./cell in order to achieve >99% deletion efficiency as determined by qRT-PCR and western blotting.

Figure S2. HIF-1α expression increases in response to EGF treatment at normoxia, and EGF prolongs HIF-1α stabilization at hypoxia. WT MTECs were either cultured in complete growth medium (containing 5% FBS + 5 μg/mL insulin + 10ng/mL EGF) or in medium supplemented with 2% FBS only for at least five passages prior to re-plating to test the effect of EGF treatment on HIF-1α expression. Cells grown to 80% confluence were incubated at hypoxia for the number of hours indicated (3, 6, 24). All cells were put into hypoxic culture beginning 24h prior to harvest of the t=0h time point, such that cells at the t=0h time point (normoxic control) were harvested at the same time as the t=24h hypoxia time point. Cells were exposed to hypoxia for the indicated number of hours prior to removal from culture and the immediate extraction of HS-WCE. HIF-1α was detected using lot E2 of NB 100-479.

Figure S3. **Histology of HIF-1α WT and KO end-stage tumors.** H&E-stained sections of end-stage (>750 mm^3) tumors derived from WT or KO cells. The WT tumors typically contained more extensive areas of necrosis than KO tumors. One representative tumor per genotype was imaged using the 5x, 20x, and 63x objectives of a Leica DM6000 upright microscope with a SPOT camera, for a final magnification of 50x, 200x or 630x, respectively. Scale bar indicates 50 μm. Digitally-scanned, whole slides of WT and KO H&E-stained tumor sections were captured using the Aperio ScanScope system; whole-slide images are posted to a public database, which may be accessed using instructions provided in the additional methods.

Figure S4. **Ki67 and activated caspase-3 immunostaining in end-stage PyMT tumors**. Paraffin-embedded, formalin fixed tissue sections from WT and KO tumors (>500-750 mm^3) were immunostained with either Ki67 or activated caspase-3 antibodies and immunoreactive complexes detected using the Vectastain ABC Elite kit and developed with DAB Impact, followed by counterstaining with Harris hematoxylin. Scale bar indicates 100 μm.

Figure S5. **Expression of p63 and ERα in WT and KO end-stage PyMT tumors**. Representative results of p63 and ERα immunostaining in WT and KO tumors (n=4/genotype), along with expression observed in normal, virgin mammary glands, which serve as the positive control (n=2 mice/~8-weeks of age, FVB strain); 200x magnification, scale bar is 50 μm. Black arrows point to examples of positive cells. No obvious changes in p63 expression or localization were detected between WT and KO tumors, whereas p63 was located basally within the virgin mammary ductal tree, as expected. No immunoreactivity for ERα was detected in end-stage WT or KO tumors (which were derived from late stage carcinomas of the MMTV-PyMT transgenic mouse), whereas almost all ductal epithelial cells in the virgin mammary gland expressed ERα, as previously reported in [77].

Figure S6. Overview of the mean fold enrichment in SFE in WT cells as compared to KO cells. A-C. Bar graphs present the mean fold enrichment of SFE ± S.E.M. for each generation (A-B, 3 biological replicates per genotype/generation) or for specific genotype/oxygen tension comparisons (C). C. The mean fold change in SFE observed for specific comparisons between genotype and oxygen tension is presented (nor, normoxia; hyp, hypoxia) (WT nor to KO nor, n=4; WT hyp to KO hyp, n=3; WT nor to WT hyp, n=5; KO nor to KO hyp, n=3). The SFE is a percentage and was determined as follows: [(the number of cells capable of forming spheres)/(total number of single cells plated) x 100].

Figure S7. HIF-1α expression in tumorspheres cultured acutely or chronically at hypoxia. WT or KO tumorspheres were originally derived from single cells plated into ultralow adhesion dishes and cultured at normoxia. A subset of WT and KO tumorspheres (80-100 μm in size) were then transferred from normoxic culture to hypoxia (0.5% O_2) for the duration of incubation, which was either acute (6h exposure) or chronic (>4 days exposure). Spheres were then isolated, HS-WCE prepared and HIF-1α expression levels were evaluated by western blotting (input of 1 μg HS-WCE/lane) using lot M1 of Novus 100-479, which produced more cross-reactive material (CRM) bands than previously observed with lot E2.

Figure S8. Gating strategy for sorting $CD133^{hi}$ versus $CD133^{neg}$ populations from mammary tumors originating in PyMT+ transgenic females. Post staining, cells resuspended in FB were subjected to flow sorting on a FACSAria machine at the UTHSC Flow Cytometry and Sorting Core. Forward and side scatter gates were set to exclude particulate debris, followed by gating for singlets based on FSC. Singlet events were determined to be viable based on gating against cells staining positive with SYTOXBlue or 7-AAD. Lin^{neg}, live, singlets were selectively gated based on the absence of expression of the mouse lineage marker panel (BD Biosciences) that was supplemented with CD31 (BD Biosciences) to exclude endothelial cells. The gating to enrich for CD133-PE^{hi} cells was manually set based on the isotype matched control antibody.

Figure S9. **Comparison of WT and KO tumor-initiating potential at day 62 post-transplant.** The percentage of FVB recipients (tumor-positive recipients/total number of recipients successfully transplanted) that developed a palpable mass of ≥5 mm in diameter was compared

on day 62 post-injection of WT or KO cells. The asterisks indicate a statistically significant difference between genotypes per cell density determined by Fisher's exact test.

Figure S10. **Mean WT and KO tumor volume in the 200 cell and 500 cell input cohorts up to day 36 post-transplant.** Comparison of mean tumor volume ± S.E.M. when 500 or 200 WT or KO cells are injected into a single cleared inguinal mammary fat pad per recipient. All recipients in the 500 and 200 cell input cohorts were euthanized on day 36 post-transplant to obtain tissue sections and RNA during the early stages of tumor outgrowth. The number of recipients with palpable masses per genotype per density is reviewed in Table 1.

Figure S11. **Mean tumor volume in the 100 cell WT and KO cohorts up to day 112 post-transplant.** Comparison of WT and KO mean tumor volume ± SEM over time when 100 cells are injected into a single cleared inguinal mammary fat pad. The decrease in mean tumor volume observed at day 112 for the 100 cell KO group is due to the euthanasia of a subset of individual recipients in this cohort bearing tumors >500 mm^3; surgical resection occurred between days 96 and 112 post-transplant.

Figure S12. **Mean WT and KO tumor volume in the 10, 25 and 50 cell input cohorts up to day 112 post-transplant.** Comparison of WT and KO mean tumor volume ± SEM over time when 10, 25 or 50 WT or KO cells are injected into a single cleared inguinal mammary fat pad. The decrease in mean tumor volume observed at day 112 for the 100 cell KO group is due to the euthanasia of a subset of individual recipients in this cohort bearing tumors >500 mm^3; surgical resection occurred between days 96 and 112 post-transplant.

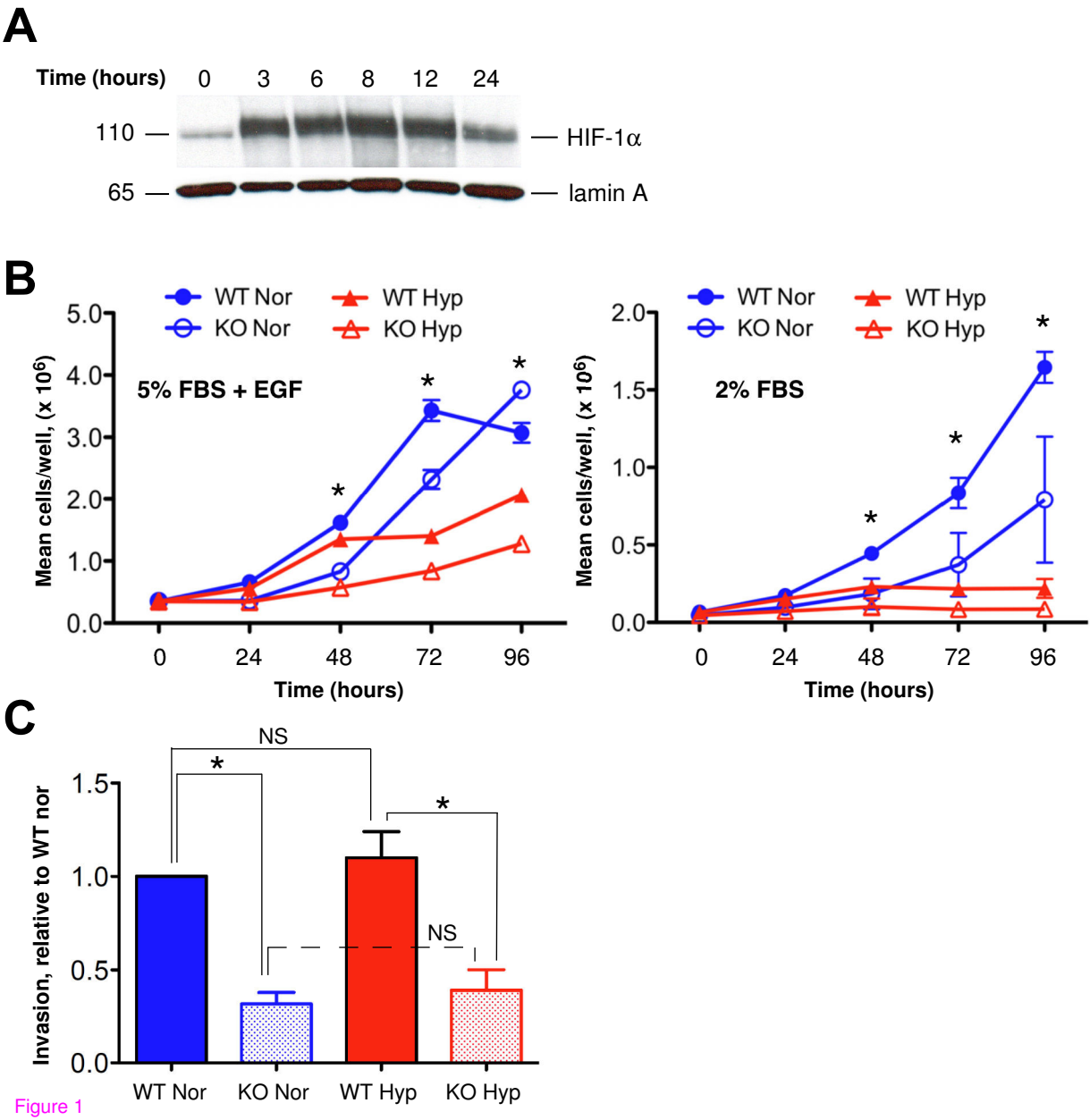
A
Time (hours) 0 3 6 8 12 24
110
65
HIF-1α
lamin A
B
WT Nor
KO Nor
WT Hyp
KO Hyp
5% FBS + EGF
Mean cells/well, (x 10^6)
Time (hours)
2% FBS
C
Invasion, relative to WT nor
NS
WT Nor
KO Nor
WT Hyp
KO Hyp

Figure 1

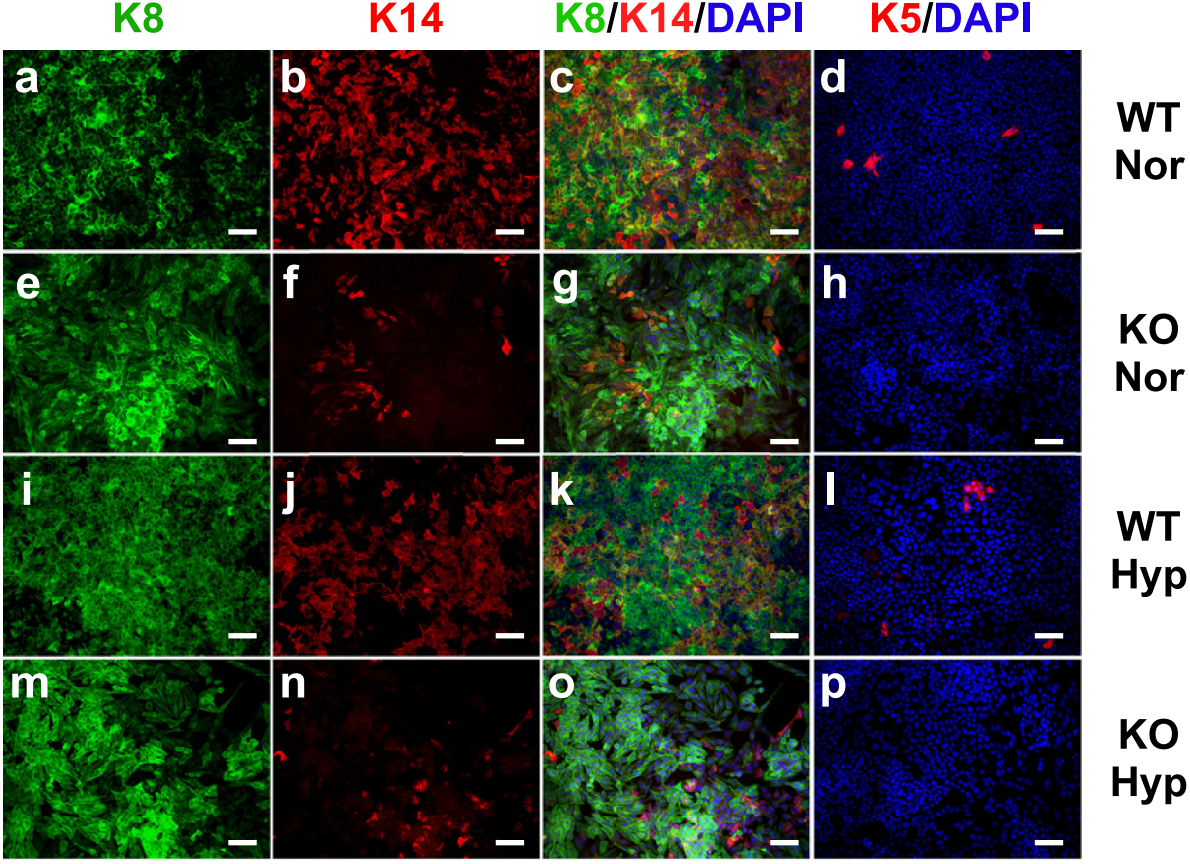
K8
K14
K8/K14/DAPI
K5/DAPI
a
b
c
d
e
f
g
h
i
j
k
l
m
n
o
p
WT Nor
KO Nor
WT Hyp
KO Hyp

Figure 2

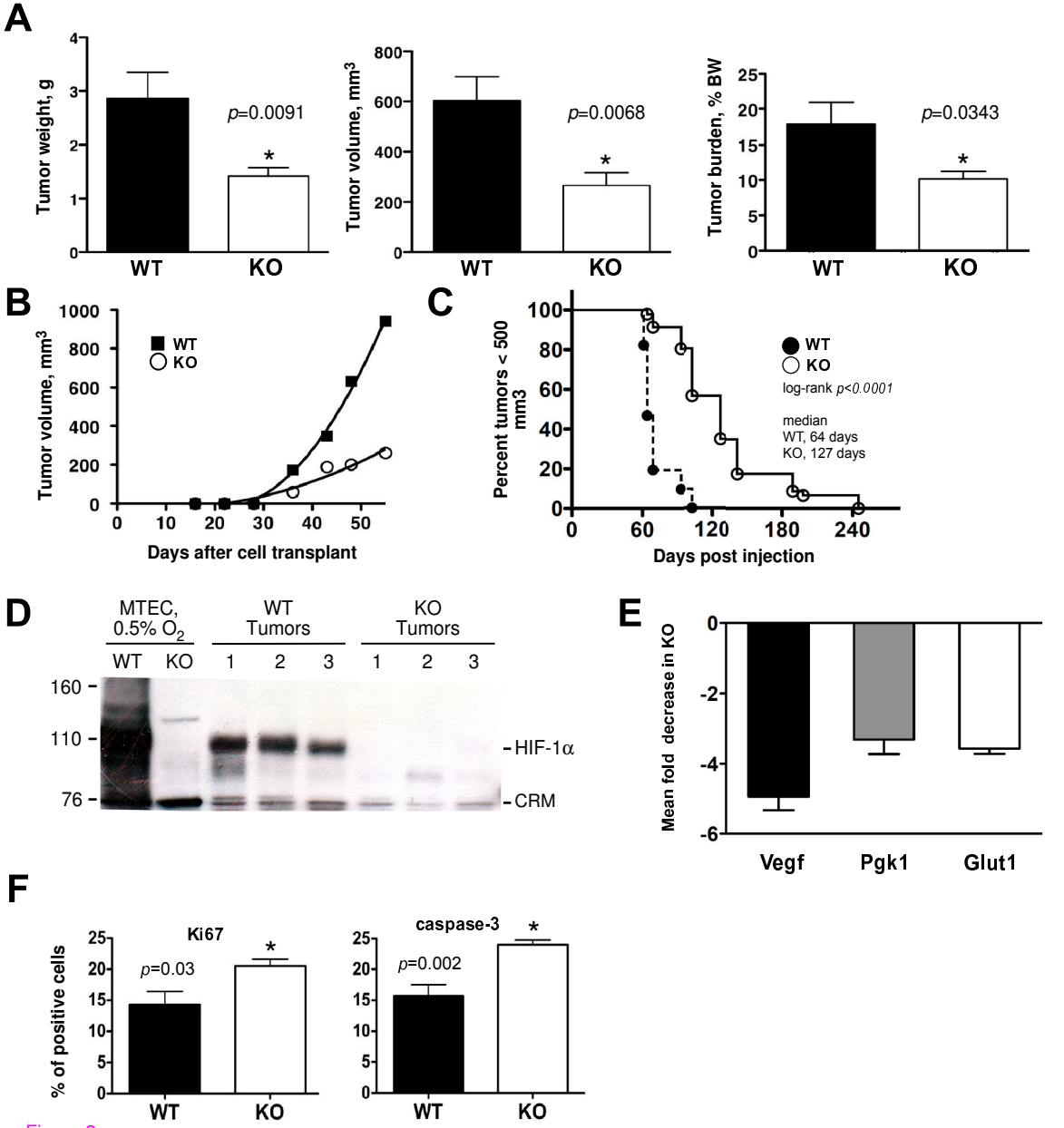
A
Tumor weight, g
p=0.0091
WT
KO
Tumor volume, mm3
p=0.0068
Tumor burden, % BW
p=0.0343
B
Tumor volume, mm3
WT
KO
Days after cell transplant
C
Percent tumors < 500 mm3
log-rank p<0.0001
median
WT, 64 days
KO, 127 days
Days post injection
D
MTEC, 0.5% O2
WT Tumors
KO Tumors
HIF-1α
CRM
E
Mean fold decrease in KO
Vegf
Pgk1
Glut1
F
Ki67
p=0.03
caspase-3
p=0.002
% of positive cells

Figure 3

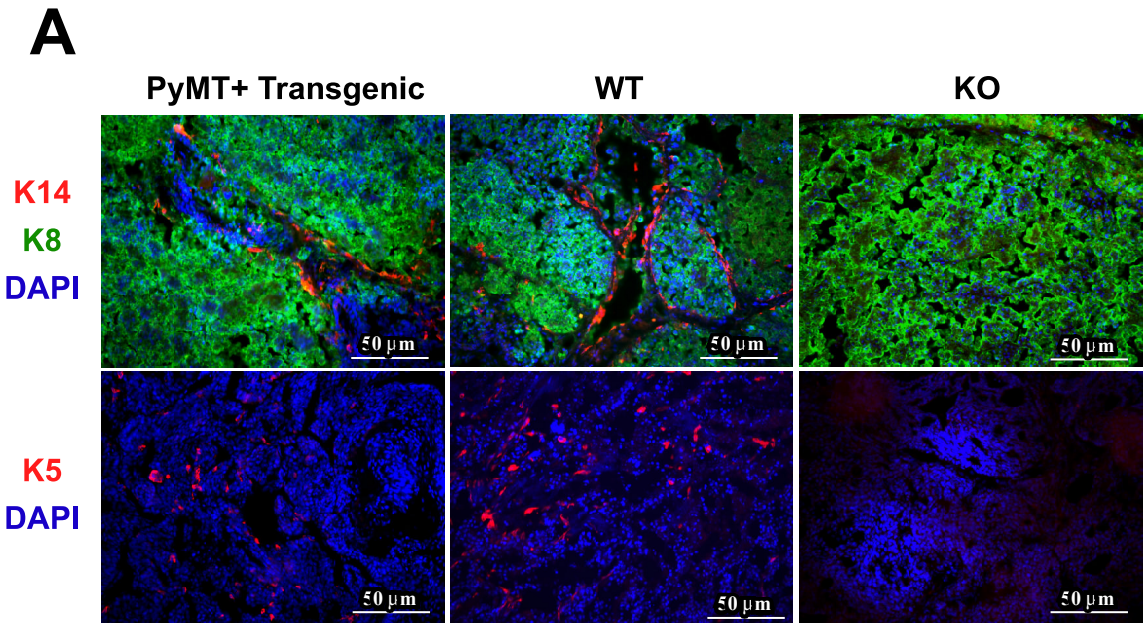
A
PyMT+ Transgenic
WT
KO
K14
K8
DAPI
K5
DAPI
50 μm
50 μm
50 μm
50 μm
50 μm
50 μm

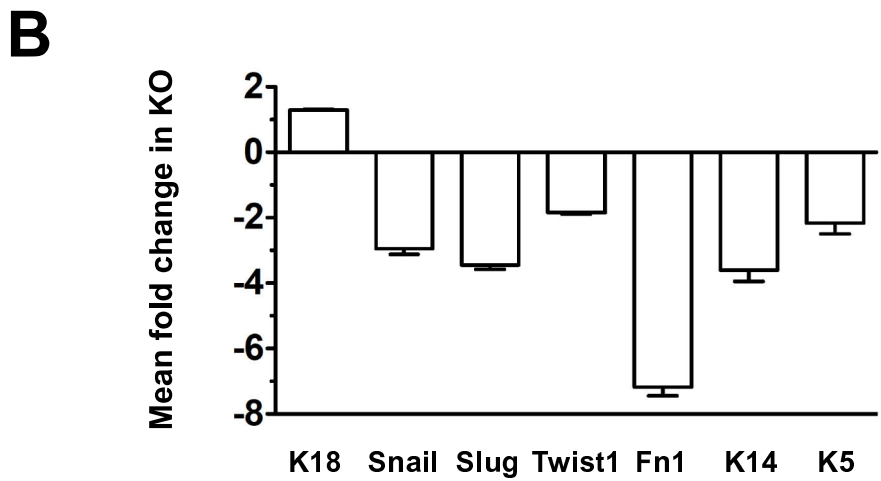
B
Mean fold change in KO
2
0
-2
-4
-6
-8
K18
Snail
Slug
Twist1
Fn1
K14
K5

Figure 4

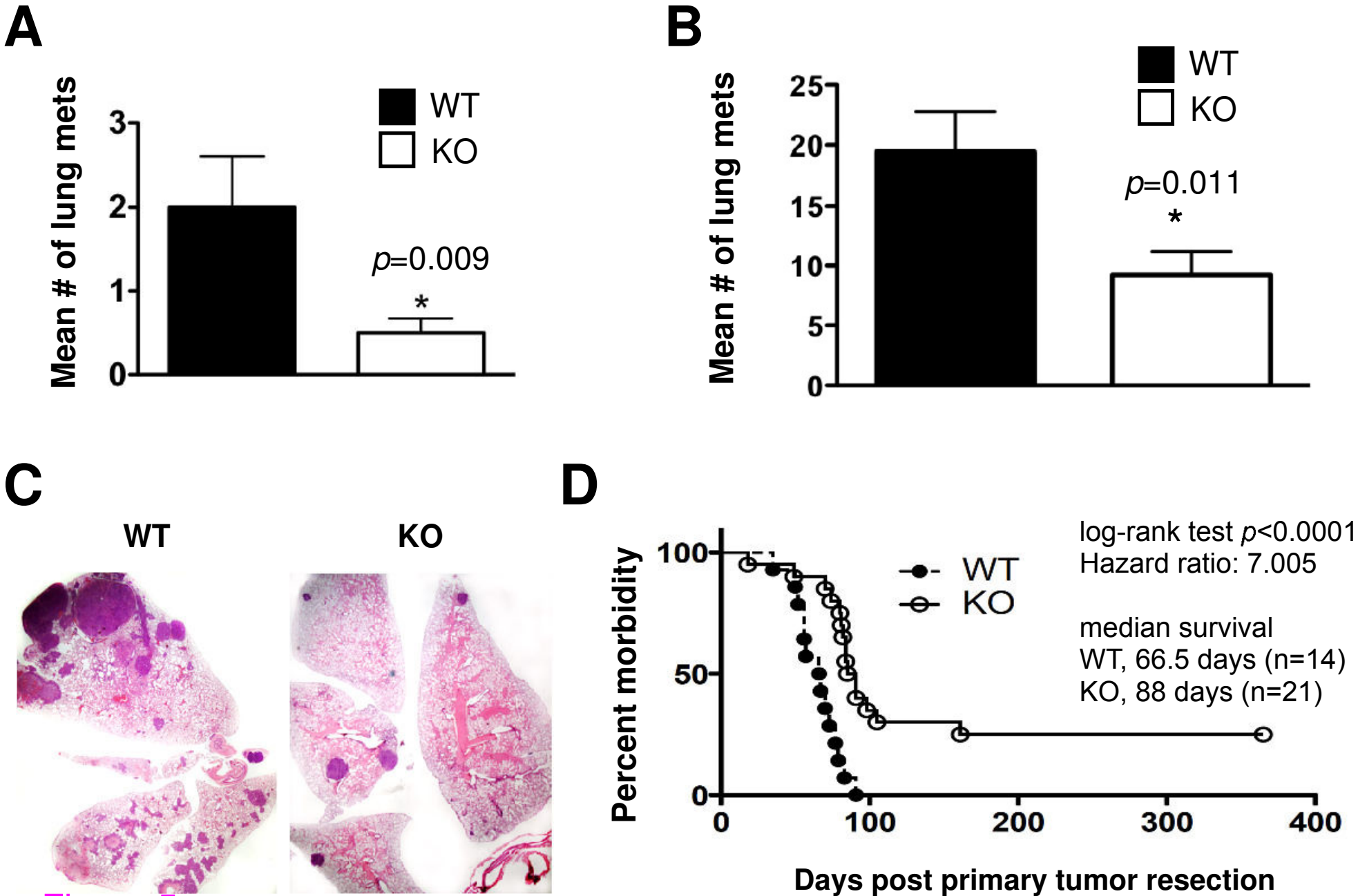
A
Mean # of lung mets
3
2
1
0
WT
KO
p=0.009
*
B
Mean # of lung mets
25
20
15
10
5
0
WT
KO
p=0.011
*
C
WT
KO
D
Percent morbidity
100
50
0
0
100
200
300
400
WT
KO
log-rank test p<0.0001
Hazard ratio: 7.005
median survival
WT, 66.5 days (n=14)
KO, 88 days (n=21)
Days post primary tumor resection

Figure 5

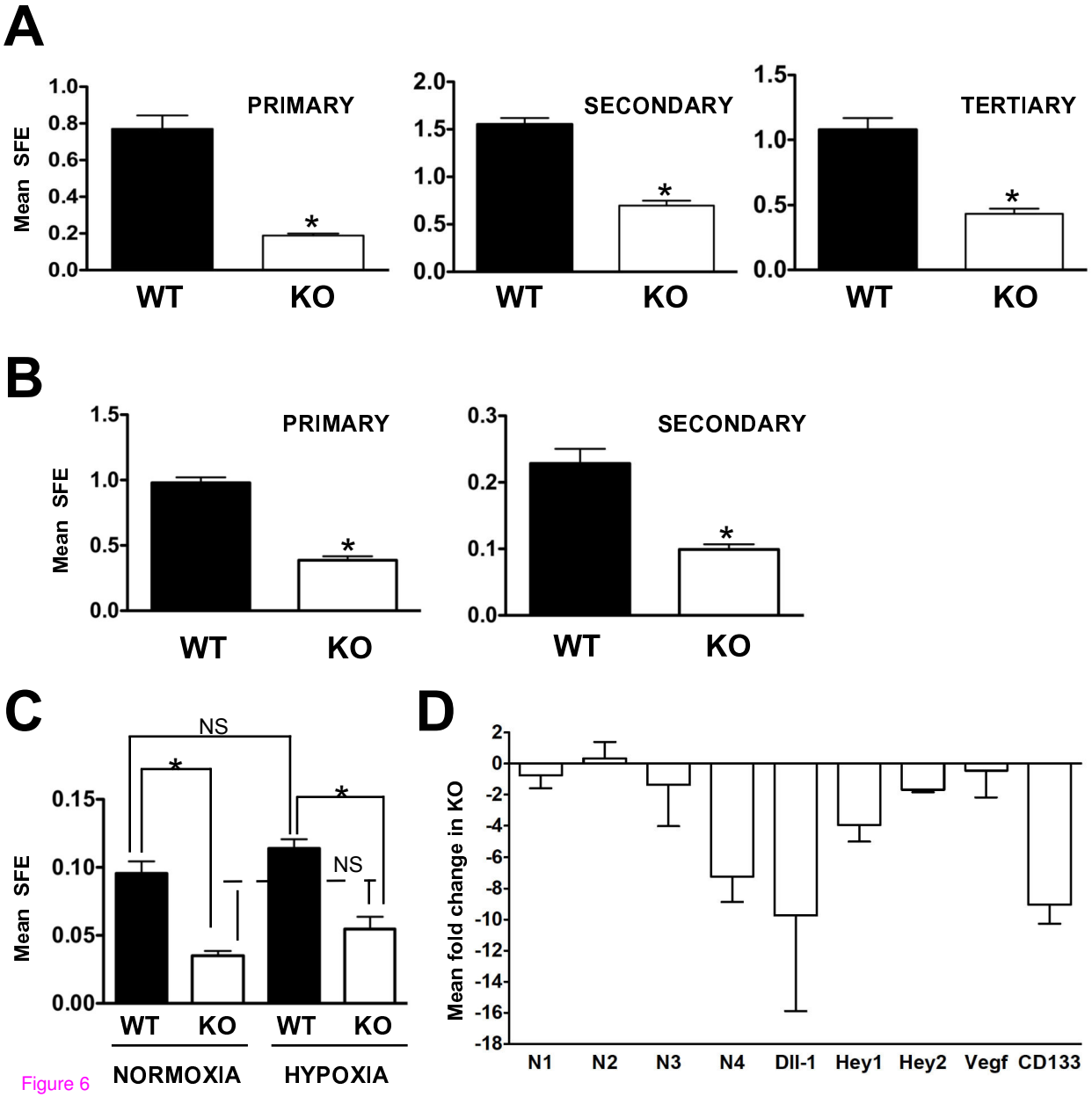
A
Mean SFE
PRIMARY
SECONDARY
TERTIARY
WT
KO
B
PRIMARY
SECONDARY
C
NS
NS
NORMOXIA
HYPOXIA
D
Mean fold change in KO
N1
N2
N3
N4
Dll-1
Hey1
Hey2
Vegf
CD133

Figure 6

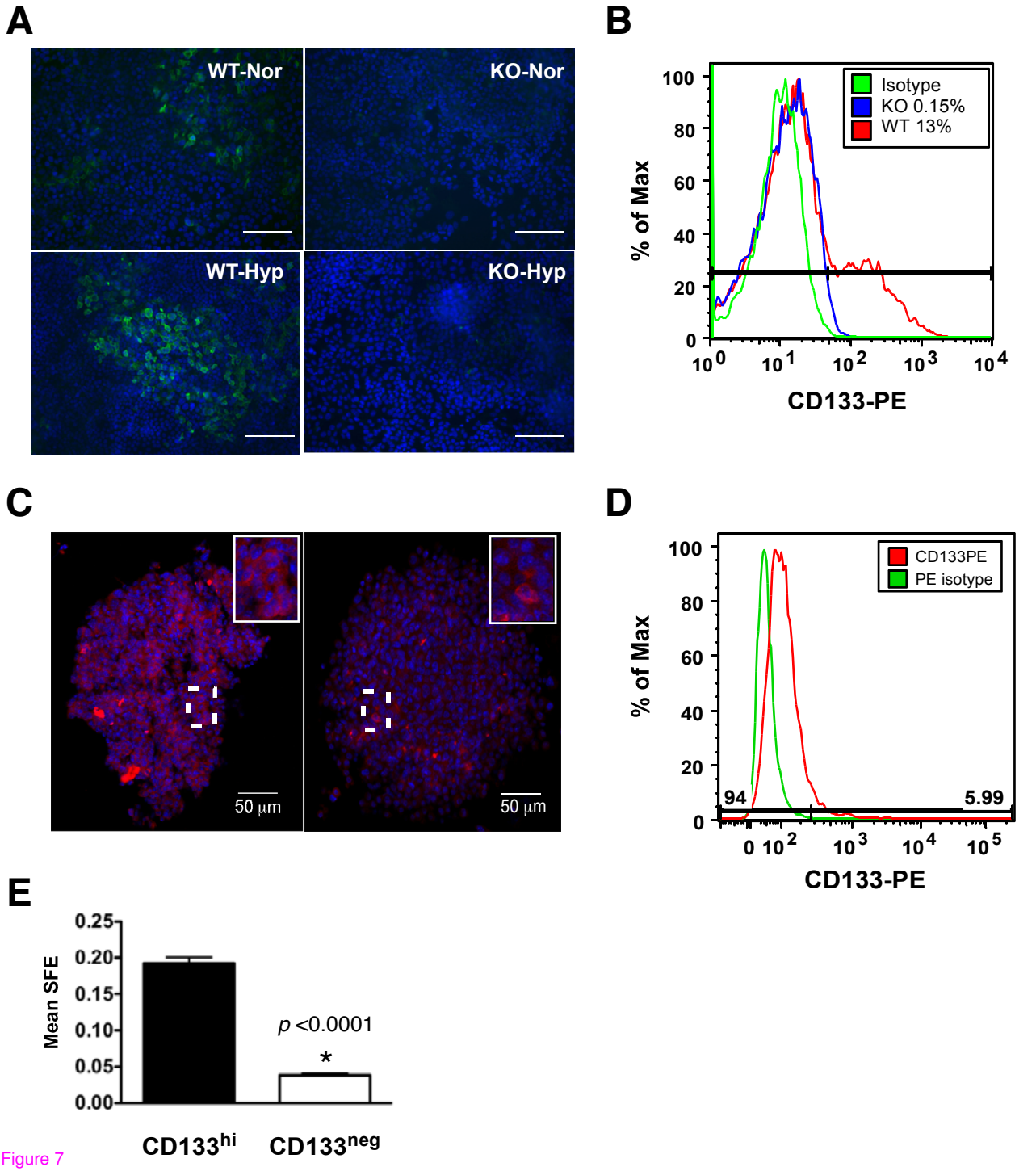
A
WT-Nor
KO-Nor
WT-Hyp
KO-Hyp
B
Isotype
KO 0.15%
WT 13%
% of Max
CD133-PE
C
50 μm
50 μm
D
CD133PE
PE isotype
% of Max
94
5.99
CD133-PE
E
Mean SFE
p <0.0001
*
CD133hi
CD133neg

Figure 7

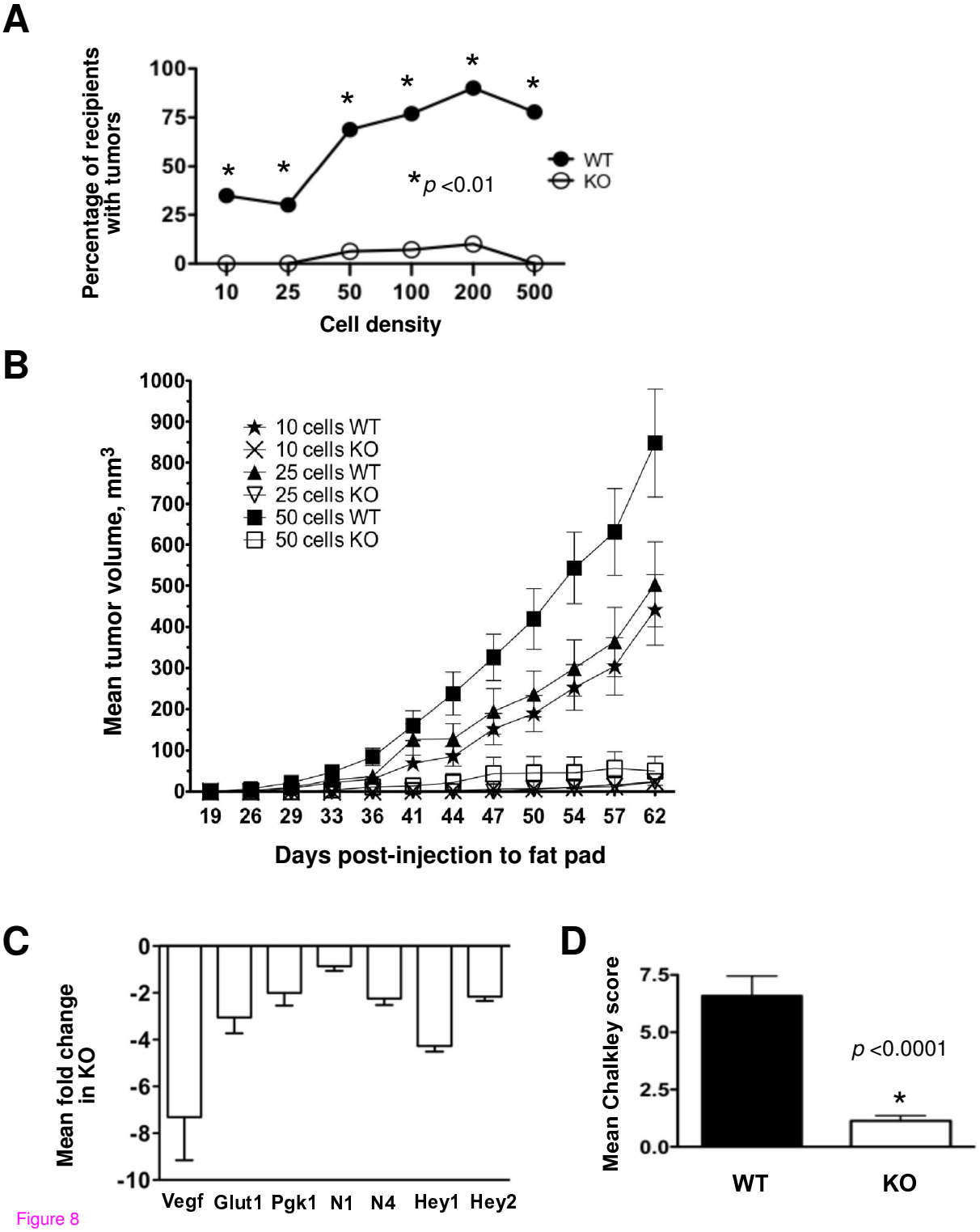
A
Percentage of recipients with tumors
100
75
50
25
0
10
25
50
100
200
500
Cell density
*p <0.01
WT
KO
B
Mean tumor volume, mm3
1000
900
800
700
600
500
400
300
200
100
0
19
26
29
33
36
41
44
47
50
54
57
62
Days post-injection to fat pad
10 cells WT
10 cells KO
25 cells WT
25 cells KO
50 cells WT
50 cells KO
C
Mean fold change in KO
0
-2
-4
-6
-8
-10
Vegf
Glut1
Pgk1
N1
N4
Hey1
Hey2
D
Mean Chalkley score
7.5
5.0
2.5
0.0
p <0.0001
WT
KO

Figure 8

Additional files provided with this submission:

Additional file 1: add file 1.docx, 14736K
http://breast-cancer-research.com/imedia/1502916071656236/supp1.docx
Additional file 2: add file 2.docx, 121K
http://breast-cancer-research.com/imedia/1326943994656237/supp2.docx